

Optimizing Urban Air Mobility: A Ground-Connected Approach to Select Optimal eVTOL Takeoff and Landing Sites for Short-Distance Intercity Travel

YANTAO WANG¹, JIASHUAI LI¹, YUJIE YUAN^{ID}¹ (Member, IEEE),
AND CHUN SING LAI^{ID}² (Senior Member, IEEE)

(Invited Paper)

¹School of Air Traffic Management, Civil Aviation University of China, Tianjin 300300, China

²Department of Electronic and Electrical Engineering, Brunel University of London, UB8 3PH London, U.K.

CORRESPONDING AUTHOR: YUJIE YUAN (e-mail: yjyuan@cauc.edu.cn).

This work was supported in part by the Fundamental Research Funds for Central Universities under Grant 3122024QD18 and in part by the funds of the National Natural Science Foundation of China NSFC under Grant 62206062.

ABSTRACT The progression of low-carbon aviation policies and the maturation of electric vertical take-off and landing (eVTOL) technology have engendered considerable prospects for the advancement of short-haul intercity and intra-city transportation systems. To harness the potential of eVTOL travel in ameliorating transportation carbon emissions and alleviating ground transportation congestion, the judicious selection of optimal eVTOL stop sites emerges as a pivotal consideration. This study delineates a framework for the delineation of intra-city and short-distance inter-city eVTOL site selection predicated on comprehensive analysis of ground transportation system interconnections. The initial phase of the framework entails the identification of potential optimal take-off and landing sites through a multi-faceted assessment of factors encompassing vehicular and passenger traffic flows, regional economic dynamics, travel behavioral patterns, and prevailing eVTOL flight regulations across heterogeneous ground transportation networks. Employing an enhanced iteration of the K -means algorithm, this phase undertakes the clustering of optimal takeoff and landing locations, thereby discerning their spatial distribution to effectively alleviate ground traffic congestion while aligning with eVTOL vertical port requirements and airspace regulatory mandates. The second phase involves the establishment of a demand gravity model to validate the optimal take-off and landing coordinate sites of eVTOL and further assess a service index indicative of traffic flow optimization. The case shows that six optimal eVTOL take-off and landing locations have been discerned by our model within the Beijing-Tianjin-Xiong'an (Hebei) region. These locations are anticipated to yield a cumulative service index of 75,465 instances, thereby efficaciously mitigating travel pressure on ground transportation infrastructure.

INDEX TERMS Urban air mobility (UAM), electric vertical take-off and landing (eVTOL), takeoff and landing sites, multi-factor site selection.

I. INTRODUCTION

As urbanization accelerates, the rise in urban population and the saturation of conventional transportation modes contribute to worsening traffic congestion. For instance, in Beijing, rushing hours from 7:00 a.m. to 10:00 a.m. have witnessed

a comprehensive travel time index of 4.04 minutes per kilometer, with an average congestion coefficient of 4.65 [1]. In London 2022, people spent an additional 156 hours on road each year due to traffic congestion [2]. In San Francisco, residents spend an average of 230 hours annually commuting

between home and work, leading to a loss of 500,000 hours of productivity [3]. Despite the robust capabilities of subway and intercity high-speed railways, their capacity are strained due to surging demand, as evidenced in prolonged crowding during peak hours in Beijing's metro and on intercity railways [4]. Moreover, the transportation sector's carbon emissions are escalating, with projections indicating a potential increase of 13 million tons in global CO₂ emissions if electric vehicles were replaced by traditional fuel vehicles [5].

Currently, there is an urgent need for a feasible solution to address the environment issue caused by traditional transportation and deal with the conflict between limited transportation resources and the continually expanding transportation demands.

Urban Air Mobility (UAM) which provides on-demand operation service for inter- or intra-urban transport is the most effective method in alleviating environmental problems, due to the use of electric vertical take-off and landing aircraft (eVTOL), which utilizes electric propulsion, the most promising technology in addressing environmental problem asserted by the Aerospace Industries Association (AIA) [6].





Besides, according to the Urban Air Mobility Market Study [7] of NASA, the UAM will be an effective way in alleviating ground transport pressure and its market is expected to become profitable in 2028, with an estimated 740 million passenger trips by aerial buses by 2030, and it is projected to handle 500 million last-mile delivery transport services by 2030 which may create billions of dollars.

Numerous countries have implemented policies to foster the advancement of UAM. Examples include the FAA's "Aviation Climate Action Plan" [8] (2021), China's incorporation of civil aviation development in its "14th Five-Year Plan" [9] (December 2022), and the European Commission's support for the "ReFuelEU Aviation" proposal [10] (April 25, 2023).

To carve out a share in the vast urban air traffic market, several industry endeavors have been undertaken to develop their eVTOL aircrafts. Successful trials have been conducted on various eVTOL models, including the Joby Aviation S4, Geely Aerofugla AE200 X01, E-Hang 216S, and Xpeng X2 (Table 1). The Joby Aviation S4, for instance, employs either a vector thrust or tilt configuration, integrating wings and vector thrusters to provide both lift and thrust. In contrast, the Geely Aerofugla AE200 X01 features a composite wing configuration, with distinct wings for lift generation and thrusters for propulsion. The E-Hang 216S and Xpeng X2, on the other hand, employ a multi-rotor configuration devoid of wings, relying solely on propellers for lift.

The foregoing discourse (Table 1) illustrates that the speed of these developed aircraft is at least 130 km/h which is 2-3 times the normal driving speed of cars in cities and thus could spare at least twice the time. Besides, as the distance between cities of short range is at most 130 km (Beijing-Tianjin; Calais-Dover; San Diego-Los Angeles are 130 km, 30 km, 120 km correspondingly), it is feasible utilizing eVTOL for short-distance intercity transport. Pertinent research also underscore the manifold advantages of eVTOL technology,

TABLE 1. The Performance of Different eVTOLs

Type	Configuration	Range (km)	Speed (km/h)	Capacity
Joby Aviation S4	 Vector thrust	161	322	4 passengers
Geely Aerofugla AE200 X01	 Composite wing	200	264	4-5 passengers
E-Hang 216S	 Multi-rotor	35	130	2 passengers or 220 kg cargo
Xpeng X2	 Multi-rotor	76	130	2 passengers

including noise reduction, environmental sustainability, and enhanced speed [11] relative to ground transportation, alongside superior safety and comfort [12] levels. Consequently, eVTOL holds substantial potential for facilitating efficient and environmentally sustainable travel.

Given the significance of eVTOL, there is a palpable need for the strategic design of infrastructure, particularly vertical take-off and landing stopping sites (vertiports), to underpin their efficient operational deployment. Different with ground transportation modes (bus, metro et al), UAM has the characteristic of high safety sensitivity, real-time response to demand and is constrained by many technological factors such as noise, airspace structure, urban terrain in low altitude. Therefore, selecting specific takeoff and landing sites for eVTOLs in urban areas is challenging yet essential.

In recent years, there has been a discernible surge in academic inquiries focused on optimizing infrastructure to accommodate the evolving paradigm of eVTOL transformative transportation modalities. Fadhil et al. [13] undertook an initial categorization of vertiports into three distinct typologies—vertipads, vertiports, and vertihubs—based on their respective spatial dimensions. Subsequently, leveraging geographic information systems (GIS) data from urban centers such as Los Angeles and Munich, they applied an analytic hierarchy process (AHP)-Delphi method to discern potential regions conducive to vertiport development, taking into account various factors including population density, vertiport layout, and noise pollution levels. These considerations were further explored by Taylor et al. [14] in their empirical investigation centered on Washington D.C. Addressing the intricate challenge of optimal location selection for vertiports, Nikhil et al. [15] formulated and resolved two distinct optimization problems—namely, capacitated and uncapacitated vertiport siting—through the employment of Mixed-Integer Programming methodologies. Meanwhile, Matthew et al. [16] approached the location selection conundrum by formulating a binary integer programming optimization model, with the cumulative time saved in commuting serving as the principal

objective function. Furthermore, Xin et al. [17] undertook a rigorous investigation into the optimal sensor placement within vertiport infrastructure, employing D-optimal criteria to identify locations that would yield the highest received signal strength. Despite the notable advancements in these studies, it is noteworthy that none have conclusively determined the precise positioning of vertiports within their respective urban landscapes.

In efforts to determine optimal vertiport locations, several studies have been conducted, each employing diverse methodologies and considerations. For instance, Jeong et al. [18] utilized population statistics from Seoul to employ the *K*-means algorithm in selecting 40 from 100 potential vertiport locations. Subsequently, they refined these selections by incorporating noise considerations. Similarly, Zhiqiang W et al. [19] utilized travel demand data from Florida to develop an Integer Programming (IP) model aimed at minimizing total cost while identifying candidate vertiport sites based on travel demand-vertiport location dynamics. Eva F et al. [20] identified two primary vertiport locations at Cologne Bonn Airport, considering legal requisites as part of their selection process, and subsequently evaluated these locations through simulated experiments. Maurilio M et al. [21] proposed a stochastic geometry-based model to address the allocation of terrestrial and aerial base stations, ensuring equitable wireless network coverage across urban and suburban areas. Conversely, Landon C et al. [22] employed five heuristic algorithms, including Elimination, Greedy, Maximal Edge-Weighted subgraph, and Greedy algorithms with updates, to address vertiport location challenges in various U.S. regions. Additionally, they investigated the interrelationships among battery range, vehicle speed, and vertiport numbers. While these studies successfully identified vertiport locations while considering factors such as travel demand and cost, they generally overlooked the specific requirements pertinent to vertiport siting.

To assess the compliance of vertical takeoff and landing (VTOL) sites with requisite standards, various factors such as the size of the vertiport, influenced by its layout and geofencing, have been thoroughly examined by Patrick B et al. [23]. Their study provided detailed insights into the infrastructure requirements of vertiports and evaluated their dimensions to ensure adequate functionality. Building upon this foundation, suitable parking arrangements for vertiports within European contexts were determined based on their respective sizes. Similarly, Brunelli et al. [24] conducted a comprehensive analysis of the impact of vertiport size on location selection. Moreover, in an effort to minimize the total distance between demand points and vertiports, he introduced a warm start technique-based *K*-means algorithm for vertiport localization, which was further refined and implemented in the algorithmic framework developed by Kai et al. [25]. In a sequential approach, Jaehyun et al. [26] initially filtered out unsuitable sites for vertiports, followed by the application of an analytical hierarchy method to discern the priority among candidate locations. Addressing the stability concerns of unmanned aerial vehicles (UAVs) during flight, Charbel H et al. [27] employed computational

fluid dynamics (CFD) simulations with an unstructured mesh to model airflow dynamics, yielding insights into the crucial role of thrust control strategies in stabilizing both thrust and altitude during UAV operations.

Given the pivotal role of vertiports in enhancing inter-modal connectivity, Jussan K et al. [28], [29] incorporated environmental constraints and integration with aviation airports into their selection process. Furthermore, Baishali R et al. [30] underscored the importance of integrating vertiports with existing transportation infrastructure. Their study developed a composite optimization model to identify optimal vertiport locations and quantities in San Francisco, with a focus on minimizing distances between vertiports and bus stations.

The aforementioned studies have predominantly focused on specific aspects such as the influence of noise, travel demand on location selection, with their aim at maximizing the revenue. However, there lies a significant vacancy in systematically analyzing the technological requirements for establishing vertiports. Ignoring the influence of technical requirements such as airspace structure, terrain, climate, grid capacity et al when selecting vertiport locations can not only disrupt the normal lives of surrounding residents but also pose a threat to the safety of eVTOL operations. For example, a lack of accurate assessment of surrounding obstacle heights and weather conditions when selecting vertiport locations can result in aircraft colliding with obstacles. Neglecting airspace constraints at selected locations can lead to eVTOLs being unable to take off and land safely. Therefore, it is of great importance to have technical restrictions thoroughly analyzed ahead of demand and revenue. The contributions of this paper are delineated as follows:

- Addressing the oversight of technical constraints during the selection process of landing and takeoff sites.
- To utilize a comprehensive model to determine the optimal location for the vertical landing site, while ensuring technical constraints. Firstly, we introduce a multi-factor screening model to eliminate areas that dissatisfied with technical constraints and identify potential demand points. Subsequently, we employ an improved *K*-means algorithm to precisely identify the optimal position for the vertical take-off and landing field.
- To develop a test model to evaluate the feasibility of eVTOL vertical takeoff and landing operations and assess their potential in alleviating ground traffic pressure.

The subsequent sections are outlined as follows. Section II provides the methodology and illustration of the proposed model. The first step, which is demonstrated in Section II Part B, is to remove the areas that dissatisfied with the technical constraints from the entire map. Secondly, various demand factors mentioned in Section II Part B (2) have been investigated to construct a thermal dynamic plot and filter the potential demand points. The third step is to determine the location of vertiports utilizing an improved *K*-means algorithm in Section II Part C. Besides, to evaluate the feasibility of vertiports, testing model in Section II Part D has been leveraged. Section III presents case studies based on data from Beijing,

Tianjin, Xiong'an (Hebei). Lastly, Section IV encapsulates the conclusions.

II. METHODOLOGY

This section presents a comprehensive model aimed at selecting and evaluating eVTOL takeoff and landing sites. A model serving potential demand to the greatest extent while ensuring safety has been proposed. The process of this model is as follows. The first step is to determine the dominant factors and remove the areas that dissatisfied with technical constraints from the map (Section B Part (1)). Then, demand points have been investigated and filtered to form a thermodynamic chart (Section B Part (2)). In the second step, an enhanced K -means algorithm is developed based on demand to identify the optimal locations for vertical takeoff and landing sites (Section II Part C). Finally, an evaluation model is applied to rigorously assess the efficiency of this location selection method and possible served demand under this vertiport layout (Section II Part D).

A. SYMBOL

The parameters involved in this article have been demonstrated in Table 2.

To ascertain the location of vertiports, factors that affect the selection problem of vertiports most need to be firstly determined. Factors considered in recent researches on this problem have been displaced in Table 3.

It can be observed from Table 3 that most of the studies concern noise & privacy, obstacle, commuting demand, available space, and transfer convenience. However, no consensus has been reached on population. Owing to the high cost of eVTOLs in the short term, to benefit from them, Fadhil D. N. [13] and Brunelli M. [24] suggest that only the high-income population should be considered, since those who have the ability to afford eVTOLs will mostly be from the high-income population. J. So [26] supposed that both permanent population—no matter their income—and floating population should be considered. To balance the service fairness for people to take eVTOL and revenue, both of income (which may be reflected by GDP of this region) and the permanent population have been considered in this research.

Moreover, few research has considered factors of congestion, transportation demand, climate and airspace. However, as an emerging mode of transportation, urban air mobility primarily aims at alleviating transportation pressure under condition where ground transportation is becoming saturated. Ignoring factors such as transportation demand and congestion condition will lead to disability in relieving transportation burden especially during peak hours. While neglecting the constraints of climate or prohibited airspace will cause eVTOL to be unable to takeoff during the majority of a year. Therefore, factors of congestion, transportation demand, climate and airspace have also been concerned in this study.

Lastly, according to “Technical Requirements of Civil Vertiports [31]” the infrastructure around vertiports should have the ability to support the operation of vertiport. Similar to

conventional aviation airport, vertiports also needs to provide essential services such as Communication, Navigation, and Surveillance (CNS), as well as maintenance and charging facilities for eVTOL aircrafts. Therefore, factors that have not been mentioned in most studies such as adequate grid power capacity and signal strength of CNS system have also been considered in this research.

In summary, factors of noise & privacy, obstacle, commuting demand, available space, transfer convenience (reflected by time to transportation hub according to the research of [16], [23], [24], [26]), congestion, transportation demand, climate, airspace, CNS signal and grid capacity have been selected as the key factors in determining the location of vertiport and will be further discussed below.

B. VARIABLE MODELING

The initial step involves removing the technical unsuitable areas and demand points based on technical criteria and demand criteria.

1) TECHNICAL CRITERIA

Although the establishment of vertiports should take the demand of a specific area into account, the complexity of urban low-altitude environment necessitates prioritizing the evaluation of whether the selected locations meet the operational conditions for eVTOL takeoff and landing to ensure their safe operation. Therefore, this article prioritizes technical constraints over demand considerations.

The technical criteria below were proposed on the basis of “Technical Requirements of Civil Vertiports [31]” and previous research [13], [14], [15], [16], [17], [18], [19], [20], [21], [22], [23], [24], [25], [26], [27], [28], [29], [30], [31] mentioned above and were demonstrated in Fig. 1. To determine whether a candidate vertiport site meets technical requirements, a binary variable (f_i) was introduced. Those whose condition dissatisfied with the following constraints will be removed from the map in advance.

Terrain constraints: Due to the need to report the utilization of land resources to local governments for verification of compliance with land use policies and regulations, the surrounding terrain such as its available size must be investigated [23], [31]. Besides, as eVTOL has to surpass urban architectural complex while takeoff and landing, the vertiports should have a good clearance condition for eVTOL to takeoff and landing safely and prevent the collision with buildings around [31]. Therefore, the height of surrounding obstacles should also be taken into account. Those areas whose available size (As_i)—acquired from Geographic Information System (GIS)—fall below a specific limitation or surrounding obstacles' height (Oh_i) lie beyond a certain requirement should be disposed as (1) and (2)

$$f_i \times As_i \geq St_{size} \quad (1)$$

$$f_i \times Oh_i \leq St_{height} \quad (2)$$

TABLE 2. The Definition of Different Parameters

Symbol	Definition (Unit)	Related in which parameter	Symbol	Definition (Unit)	Related in which parameter
As_i	The available size of region i (m^2)	Terrain	n_i	The amount of road sections in region i	Congestion
At_i	Additional transport time in region i (min)	Congestion	Oh_i	Obstacles' height in region i (m)	Terrain
Atr_i	Attractive index multiplied by W_i and VP_i	Demand density(D_i)	P_c	The power needed to charge a single eVTOL (kW)	Grid capacity
B_i	GDP value in district i (billion CNY)	Service demand(P_d)	P_e	The commercial electricity price in China (CNY/kWh)	Ticket price
Cd_i	The commuting demand in region i (count)	Commute demand	P_i^{ag}	The available grid power in region i (kW)	Grid capacity
Cg_i	The congestion coefficient of road section i	Congestion	P_c	The total grid power (kW)	Grid capacity
D_i	The total demand density in i (count/ km^2)	Demand density	P_u	The grid power that has been utilized (kW)	Grid capacity
d_{ij}	The great circle distance between vertipoint i and j (km)	Service demand	P_s	The grid power needs to be reserved(kW)	Grid capacity
d_1	Distance from vertipoint candidate sites to residential buildings (m)	Noise	P_i	The amount of people in region i (count)	Population
d_2	The wingspan of eVTOL (m)	Noise	P_{in}	The input power of the selected region(kW)	Grid capacity
Ed_{ij}	The Euclidean distance of i and j	Attractive index	P_{pg}	The power generated in the selected region(kW)	Grid capacity
e	The error of this proposed method	Error	Pd_{ij}	Passenger served between vertipoint i and j (count)	Service demand
f_i	A binary variable which equals 1 if the candidate site is selected, 0 otherwise.	Vertipoint location	p_i	The number of residents live in district i	Population
F_i	The passenger flow of transportation hub i (count)	Transportation demand	r	The radius of the specific demand area (km)	Demand density
g	The generative variable in gravity model	Demand density	rt_i	The ratio of additional travel time to unblocked travel time	Congestion
k	Optimal vertipoint amount (count)	Output parameter	S	The size of specific area(km^2)	Congestion
imp	The impedance variable in gravity model	Service demand	Sr_i	The signal reception strength in region i	CNS
L_{max}	The aircraft's maximum noise (dB)	Noise	St_i	Standard i to evaluate whether a demand point or vertipoint should be excluded	Demand density
L_{en}	The noise produced by the environment (dB)	Noise	T_i	Sum of passenger flow in transportation stations of region i (count)	Transportation demand
L_1	The noise experienced by residents (dB)	Noise			

TABLE 2. Continued.

Symbol	Definition (Unit)	Related in which parameter	Symbol	Definition (Unit)	Related in which parameter
Td	Total ground pressure eVTOL alleviates under this vertiport layout	Service demand	Wt_i	Walking time to the transportation stations locating near vertiports (min)	Transfer convenience
t_{ij}	The ticket price from vertiport i to j (CNY)	Ticket price	Wf_i	The Beaufort scale wind force in region i	Climate
Ub_i	The unblocked transport time on road section i (min)	Congestion	x_i	The longitude of vertiport	Output parameter
VP_i	The amount of passenger visiting scenic spots that locate in region i (count)	Tourism demand	y_i	The latitude of vertiport	Output parameter
Vis_i	The visibility in region i (m)	Climate	α, β, C	Coefficients of gravity model which could be computed by least square method	Service demand
W_i	The amount of people working in region i (count)	Commuting demand	γ_i	Weight of demand i in the total demand.	Demand density

TABLE 3. Factors Considered in Recent Researches

Research	Factors									Transfer time to Transportation hub
	Airspace	Noise & Privacy	Congestion	Climate	Obstacle	Population	Commuting Demand	Transportation demand	Available space	
Fadhil D. N ^[13]	×	✓	×	×	×	✓	✓	✓	×	✓
Daskilewicz M ^[16]	×	×	×	×	×	×	✓	×	×	✓
Jeong J ^[18]	×	✓	✓	×	×	×	×	×	×	×
Bruesberg p ^[23]	✓	✓	×	×	✓	×	×	×	✓	✓
Brunelli M ^[24]	✓	✓	×	✓	✓	✓	✓	×	✓	✓
J. So ^[26]	×	✓	✓	✓	✓	✓	✓	✓	✓	×
Rahman B ^[30]	×	×	×	×	✓	✓	✓	✓	✓	✓

The vertiport containing a 23 m pad is a square with sides of 30 m in length [23]. Besides, according to the document published by EASA [32], vertiport has three kinds of takeoff procedure: Elevated Conventional Takeoff (EConvTO), Conventional Takeoff (ConvTO), Vertical Takeoff (VTO), while the VTO is recommended for the operation of urban city. A 30.5 m vertical take-off altitude is required in VTO takeoff procedure before climbing [31] (Fig. 2) and the obstacle surface within 100 m cannot exceed 12.5 m above the elevation height [23]. Therefore, the position where vertiport locates should have at least 900 m² in size ($St_{size}=900$ m²), and the obstacles around cannot exceed the platform by 43 m ($St_{height}=43$ m).

Noise (DB_i): In order to avoid disrupting the normal lives of surrounding residents [18], the noise level experienced by residents around the takeoff and landing sites must be

considered [31]. In this study, noise is calculated through (3), where L_{max} is the maximum noise eVTOL could produce; d_1 is the wingspan of eVTOL and d_2 is the distance from candidate sites to residential buildings, hospitals, sanatoriums nearby. If the noise levels experienced by residents exceed the requirements set by various governments regarding commercial noise emission standards (St_{noise}), which is 75 dB in China [33] and 65 dB according to NASA [34], the candidate vertiport site should be abandoned as (4) illustrates.

$$L_1 = \max \left\{ L_{\max} - 20 \log_{10} \left(\frac{d_2}{d_1} \right), L_{en} \right\} \quad (3)$$

$$f_i = \begin{cases} 1 & L_1 \leq St_{noise} \\ 0 & \text{otherwise} \end{cases} \quad (4)$$

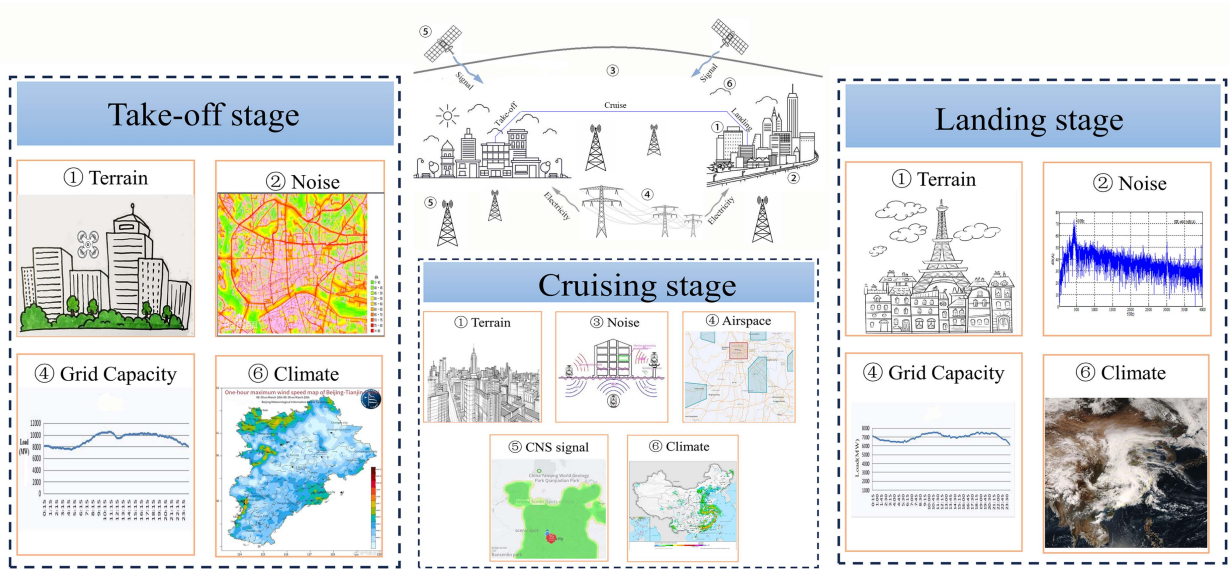


FIGURE 1. Technical constraints considered in this work.

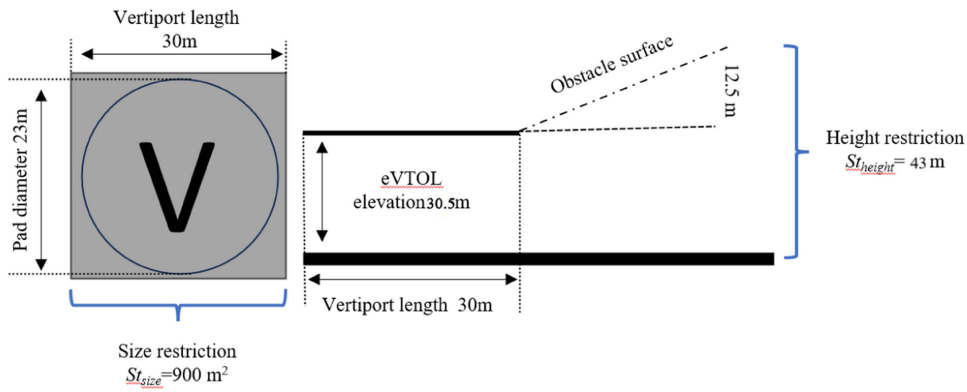


FIGURE 2. The layout of an eVTOL take-off and landing pad and the size and requirements of a single pad vertiport [23], [32].

Airspace constraints: Considering the prohibited (Prh) and restricted (Res) zones that protect government departments and military secrets, which may intersect with the eVTOL operating area in low-altitude airspace, it is necessary to account for airspace structure when identifying vertiport locations. Although some restricted zones do not constrain aircraft from entering at all times, to maximize the operational duration of eVTOLs for revenue generation, it is crucial to consider these zones. Therefore, if the chosen area overlaps with any restricted or prohibited zones, it should be eliminated from consideration (5).

$$f_i = \begin{cases} 1 & (x_i, y_i) \notin (Prh \cup Res) \\ 0 & \text{otherwise} \end{cases} \quad (5)$$

In addition, according to documents released by CAAC [35], airspace above 300 m will be entirely used for low-altitude economic development and eVTOL operations. How to grid this airspace to maximize utilization efficiency while ensuring safe distances between eVTOLs is an issue that is independent of the vertiport sites selection and is equally

important as site determination. Thus, the issue of airspace planning has not been considered in this study.

Grid power limitation: As it was demonstrated in [31], [36], the vertiports should be equipped with maintenance and charging facilities for the arriving eVTOLs. Therefore, to ensure that the eVTOL could be charged at vertiports, the grid should accommodate at least one eVTOL for its charging behavior (6). The available grid power P_i^{ag} can be acquired through subtracting the total grid power P_G from the power utilized P_u and the power that needs to be reserved for safety concerns P_s which is 5% of the total capacity [36] (7). Herein, the total grid power P_G can be calculated by adding the annual power generation P_{pg} with the input power P_{in} in this region (8). These data could be available after the negotiation with local governments.

$$P_i^{ag} \geq P_c \quad (6)$$

Where:

$$P_i^{ag} = P_G - P_u - P_s = 0.95P_G - P_u \quad (7)$$

TABLE 4. The Value of Technical Standards Related in Vertiport Selection

Standard (St_i)	Value
St_{size}	900 m ²
St_{height}	17 m
St_{noise}	75/65 dB
St_{signal}	33 dBm
$St_{visibility}$	1,219/1,000 m

$$P_G = P_{pg} + P_{in} \quad (8)$$

CNS constraints: Due to the complex terrain, and variable weather conditions in urban low-altitude areas, a high-precision communication navigation and surveillance (CNS) system is needed to monitor eVTOL dynamics and surrounding environmental conditions continuously and stay connected. However, CNS system signals could be blocked by the buildings in urban areas, and there is a significant amount of interference from broadcasting and mobile signals [31], [37]. Therefore, before establishing a takeoff and landing site ($f_i=1$), it is essential to ensure that the minimum signal reception strength Sr_i within a year at that point is higher than a certain threshold. According to the survey of M. Cen Ertürk et al. [38], to ensure the communication connectivity between eVTOL and vertiports, 33 dBm transmitter output power and 43.2 dBi transmitter antenna or a 39.7 dBi receiver antenna will be required ($St_{signal}=33$ dBm).

$$Sr_i \geq f_i \times St_{signal} \quad (9)$$

Climate restriction: Similar to aviation aircraft, eVTOL also has a high requirement on wind and visibility [31]. Strong wind or low visibility can easily cause eVTOLs to deviate from their intended flight path, posing a safety threat. Therefore, it is essential to investigate the visibility and Beaufort scale (an index to reflect wind force) in the selected area over the past month before establishing a vertiport. According to the documents [32], [39] published by FAA and EASA the required visibility ($St_{visibility}$) for eVTOL to take-off and landing is at least 1219 m, 1000 m correspondingly. Area whose annually minimum visibility dissatisfied with the visibility requirement needs to be disposed.

$$Vis_i > f_i \times St_{visibility} \quad (10)$$

$$f_i \times Wf_i < St_{wind} \quad (11)$$

The standards mentioned above were further demonstrated in Table 4.

2) DEMAND CRITERIA

In the second step of this model, in order to determine the location of vertiports, a thermodynamic chart has been developed to reflect the distribution of these demands (commuting and tourism) and transport conditions such as congestion condition, passenger flow of transportation hubs et al. In the process of developing this thermodynamic chart, all the scenic spots, Central Business District (CBD), transportation hubs et al are deemed as demand generation points (12). However,

since the demand at a specific point may consist of both the local demand and the demand from nearby areas, it is necessary to define a circular area R_i with a radius r to accurately calculate the total demand [40], [41], [42] (13). For places that locate beyond this circle will have no demand contribution to this demand generation point. In this article, an attractive function (Atr), which reflects the demand composition within this area, was designed according to [39] as (14) illustrates where Ed_{kc} is the Euclidean distance between the place and the centroid of R_i , which is also the demand generation point.

$$R_i = \{Cd_i, Td_i, Ti, Pi\} \quad (12)$$

$$S = \pi \times r^2 \quad (13)$$

$$Atr = \begin{cases} 1 & Ed_{kc} \leq 50 \\ 0.75 & 50 < Ed_{kc} \leq 100 \\ 0.5 & 100 < Ed_{kc} \leq 150 \\ 0.25 & 150 < Ed_{kc} \leq 200 \\ 0 & Ed_{kc} > 200 \end{cases} \quad (14)$$

After determining the demand composition of this demand generation point, various demand could also be investigated and calculated.

Commuting demand (Cd_i): As mentioned earlier, urban ground traffic experiences enormous passenger flow during morning and evening peak hours, thus commuting demand has been introduced into this model. In this research, a commuting demand is regarded to generate only if the commuter works within the specific area of a certain demand generation point mentioned above.

$$Cd = \{Cd|W_i \in R_i\} \quad (15)$$

However, as only represent the amount of people who works in this region (W_i) can be obtained from the platform, thus a ratio is needed to estimate the commuting demand based on its distance to the centroid of R_i and (14). The commuting demand (Cd_i) within this area (R_i) could be calculated leveraging (16)

$$Cd_i = \sum W_i \times Atr_i (W_i \in R_i) \quad (16)$$

Tourism demand (Td): It is also essential to take tourism demand into account especially during holiday, due to the huge number of tourists. Similar with commuting demand, tourism demand is established when scenic spot locates within the specific area.

$$Td = \{Td|VP_i \in R_i\} \quad (17)$$

Owing to the same reason mentioned in commuting demand, tourism demand (Td) was acquired through multiplying the tourist flow in scenic spots (VP_i) collected from platform by a ratio Atr_i according to its distance to the centroid of R_i as (18) demonstrates.

$$Td_i = \sum VP_i \times Atr_i (VP_i \in R_i) \quad (18)$$

Transportation demand: To enhance the inter-model connectivity and make it convenient to transport, the volume of

passenger flow of some important transportation hubs (T_i) such as metro station, railway station, airport et al were introduced into this model. The passenger flow of transportation hub (T_i) in this article was computed by accumulating the flow of transportation hub (F_i) within the selected area R_i (19).

$$T_i = \sum F_i \times Atr_i (F_i \in R_i) \quad (19)$$

Population (P_i): Population has a great impact on the size of market eVTOL operates, therefore, population of different regions are considered [19]. Population (P_i) is the total number of residents in all administrative districts (p_i) within this area.

$$P_i = \sum p_i (p_i \in R_i) \quad (20)$$

Transfer convenience: Moreover, to ensure optimal accessibility for passengers transitioning between eVTOL and other transportation modes, careful consideration must be given to the walking time (Wt_i) from vertiports to transportation stations. Vertiports exceeding a predefined threshold in terms of walking time (St_{time}) acquired through Opinion Poll, to the nearest transportation station, as specified by (21), warrant appropriate disposal measure [41].

$$(1 - f_i) \times Wt_i \geq St_{time} \quad (21)$$

Congestion Condition: As mentioned in Section I, UAM has great potential in alleviating ground traffic burden, to better leverage its effectiveness and mitigates the pressure of ground transportation especially in rushing hours, additional transport time (At_i) has been introduced to reflect the congestion condition of each road section. The additional transport time is calculated as follows.

- 1) *Average the congestion coefficient of roads:* Given that congestion index serves as a straightforward parameter reflecting road congestion conditions and is easily obtainable. The congestion coefficient was employed in this research to indicate the level of pressure on ground transportation. Then the congestion coefficient of each road section is collected and summed altogether to acquire the sum of congestion coefficient which is further divided by the amount of road section n_1 as (22). The variable $Aver_i$ obtained in (22) was utilized to represent the congestion coefficient of the selected area.

$$Aver_i = \frac{\sum_{i=1}^{n_1} Cg_i}{n_1} \quad (22)$$

- 2) *Calculate the additional transport time:* Based on the average of congestion coefficient ($Aver_i$) and Table 5 [43], [44], the ratio of additional travel time to unblocked travel time (rt_i) can be obtained. Through multiplying rt_i with the unblocked travel time (Ub_i), which can be acquired from map software such as Google Maps and Amap et al, the additional travel time within this region can be gained (23).

$$At_i = rt_i \times Ub_i \quad (23)$$

TABLE 5. The Relation Between Congestion Coefficient and the Ratio of Additional Travel Time to Actual Travel Time

Congestion coefficient	the ratio of additional travel time to unblocked travel time(rt_i)
0~2	0
2~4	0.2~0.5
4~6	0.5~0.8
6~8	0.8~1.1
8~10	>1.1

After compiling the amount of various demand, Analytic Hierarchy Process (AHP) method is utilized to evaluate the weight γ of each demand factor and formulate a formula to integrate these parameters into a single demand variable [13], [24] to plot the thermodynamic chart with each demand generation point as a demand point.

The equation to calculate the demand density of a potential demand point considering variables mentioned above was demonstrated in (24) [14], [25], where γ implies the weight of variable in the total demand.

$$D_i = \frac{(P_i \times \gamma_p + T_i \times \gamma_{Td} + Cd_i \times \gamma_{Cd} + At_i \times \gamma_{At})}{S} \quad (24)$$

As vertiport is an airport designated for eVTOL to transport passenger, thus only when a potential demand point whose total demand density (D_i) lies above a certain standard (St_{demand}) can a vertiport be established around. The potential demand points with their values demand density inconsistent with (25) will be excluded.

$$D_i \geq St_{demand} \quad (25)$$

C. ALGORITHM DESIGN

A modified K -means algorithm, which incorporates the Broyden-Fletcher-Goldfarb-Shanno (BFGS) method [45], was developed using the filtered demand points' longitude and latitude coordinates as input parameters. This approach aims to identify vertiport locations, thereby reducing the need for additional time-off from passenger travel services when using eVTOLs, while maximizing the Euclidean distance between vertiports to expand the service area. Although this could also be achieved through K -means algorithm as the cluster number k and the lon-lat coordinates of the demand points are fixed. Owing to lack of initial optimal clustering of these demand points, the K -means clustering algorithm can have multiple results.

As demonstrated in Fig. 3 to exercise this algorithm, the optimal number of clusters k , which is also the optimal number of vertiports, needs to be ascertained firstly. Assume that $\{\lambda_1, \lambda_2, \dots, \lambda_n\}$ represents the lon-lat vector coordinates of the demand points filtered by (25) and (29). The vector coordinates of several cluster centroids, $\{\mu_1, \mu_2, \dots, \mu_k\}$, represent the locations of vertiports. The optimal number of clusters k was determined using the elbow method, which minimizes the sum of squared errors (SSE) where SSE is calculated as the sum of squared distances from each demand

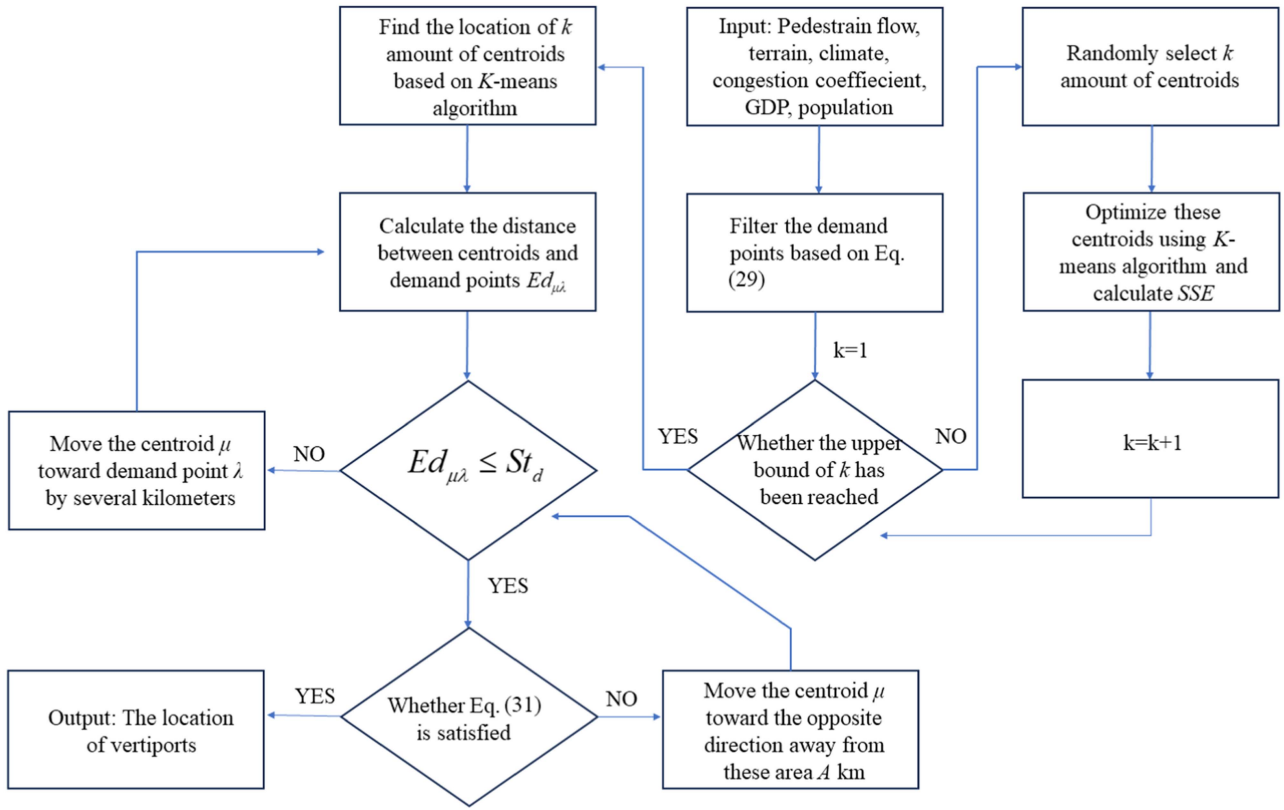


FIGURE 3. The flowchart of this proposed algorithm.

TABLE 6. Algorithm of Elbow Method

Algorithm: the optimal number of vertiports
Step 1: Determine the lon-lat coordinates matrix of demand points Compute the demand density(D_i) of each demand points, if $D_i \geq St$ add the lon-lat coordinate of the demand point into the matrix.
Step 2: Identify the location of cluster centroids μ for $k \in$ the range of k do Acquire the location of cluster centroids through K -means algorithm end for
Step 3: Identify the optimal number of k for $k \in$ the range of k do Calculate the square of Euclidean distance between demand point λ and the vertipoint μ under different k end for
Find the minimum value of SSE and its corresponding k .

point to its assigned vertipoint cluster ω , as shown in (26) and (27). Where $\|\vec{\lambda} - \vec{\mu}(\omega_k)\|$ is the Euclidean distance between demand point λ and its assigned vertipoint μ . The pseudo code is demonstrated in Table 6.

$$k = \min SSE \quad (26)$$

$$SSE = \sum_{k=1}^K \sum_{\vec{\lambda} \in \omega_k} \|\vec{\lambda} - \vec{\mu}(\omega_k)\|^2 \quad (27)$$

Take k and the lon-lat coordinates of these filtered demand points as input, a feasible cluster and its corresponding

geometric centers—which are also the position of candidate vertipoints—were selected arbitrarily from the results of K -means algorithm. To maximize vertipoints service area and make it convenient for passenger to travel, (28) and (30) have been established. As K -means algorithm utilizes maximizing the distance between different cluster centroid μ , therefore, the distance between vertipoints μ and demand points λ (30) is the only distance constraint considered in this algorithm as Fig. 3 demonstrates. Those centroids μ whose distance from demand points λ lies beyond a certain distance St_d will be moved towards the demand point within cluster ω that has the longest distance from μ by several kilometers until (30) is satisfied (Fig. 3).

Once the vertipoint sites are fixed, the framework solves a set of BFGS problems with vertipoints' longitude and latitude coordinates serving as input parameters to meet the technical constraints (31). If the solution of BFGS problems dissatisfies the technical constraints, the algorithm will search towards the regions that meet the technical constraints.

The optimization problem is written as follows:

$$\left\{ \max_{\mu \in \omega_1} \sum_{\mu \in \omega} Ed_{\mu\mu_1}, \min_{\lambda, \mu \in \omega} \sum Ed_{\mu\lambda} \right\} \quad (28)$$

Subject to:

$$\lambda \in \{\lambda | D_{\lambda} \geq St_{demand}\} \quad (29)$$

$$Ed_{\mu\lambda} \leq St_d \quad (30)$$

$$\begin{aligned} \mu \in \omega \cap \{As_\mu \geq St_{size}, Oh_\mu \leq St_{height}, E_\mu^{ag} \geq E_r, Sr_\mu \\ \geq St_{signal}, \\ Vis_\mu > St_{visibility}, Wf_\mu < St_{wind}\} \end{aligned} \quad (31)$$

Where:

$$Ed_{\mu\lambda} = \|\lambda - \mu\| \quad (32)$$

The computational complexity of this developed algorithm is related to its cluster amounts, iteration times, the number and dimension of parameters according to [46].

The flow chart of the developed algorithm is displaced in Fig. 3.

D. CONSTRUCTION OF EVALUATING MODEL

1) SERVICE DEMAND FORECASTING MODEL

A forecasting model has been constructed to calculate the service passenger (Pd_{ij}) between two spots and quantify the extent to which eVTOL mitigates ground transportation pressure, shown as (33).

$$\ln Pd_{ij} = \ln C + \sum (\alpha_i \times \ln g_i) - \sum (\beta_i \times \ln imp_i) \quad (33)$$

As GDP reflects the income and wealth of this region, it has a positive effect on total passenger demand. Therefore, g_i utilized in (33) is the GDP product of district i and j where two vertiports locate [47]. Besides, the passenger demand is also negatively affected by the ticket price and distance between vertiports. Thus, the impedance variable (imp_i) in (33) is ticket price and distance. Ticket price in gravity model was estimated [48] based on (34). The distance (d_{ij}) was calculated leveraging Haversine formulation (35)-(39) based on the lon-lat coordinates of vertiports in this study.

$$t_{ij} = (2 \times 10^{-4} \times P_e + 0.0653) \times d_{ij} + 140 \quad (34)$$

$$dlat = lat(j) - lat(i) \quad (35)$$

$$dlon = lon(j) - lon(i) \quad (36)$$

$$\begin{aligned} a = \sin\left(\frac{dlat}{2}\right)^2 + \cos(lat(i)) \times \cos(lat(j)) \\ \times \sin\left(\frac{dlon}{2}\right)^2 \end{aligned} \quad (37)$$

$$c = 2 \times \arctan(\sqrt{a}) \quad (38)$$

$$d_{ij} = 6371 \times c \quad (39)$$

The forecasting model (33) considering these variables [45] can be further illustrated as (40).

$$\begin{aligned} \ln Pd_{ij} = -6.73 + 0.41 \ln B_{ij} - 1.09 \ln t_{ij} - 0.34 \ln d_{ij} \\ + 0.78A_{ij} \end{aligned} \quad (40)$$

2) TESTING MODEL

To evaluate the feasibility of the identified vertiport locations, a testing model was developed based on surrounding terrain parameters, including available area dimensions, obstacle heights, and walking distances from vertiports to other transportation stations. Additionally, a demand matrix was integrated into this model to quantify passenger demand between different vertiports in the proposed layout. This enabled the estimation of the total alleviation of ground transport pressure (Td) by summing all elements in the demand matrix, as specified in (41).

$$Td = \sum_{j=1}^k \sum_{i=1}^k Pd_{ij} \quad (41)$$

Besides, (42) has also been utilized to validate the precision of this proposed method. Herein, $d_{ii'}$ is the average distance deviation between the vertiports obtained in case study i and validation case study i' ; k is the optimal amount of vertiports in validation case study and e , the error of this method, is set as the average of distance deviation in all validation case studies.

$$e = \frac{\sum_{i=1}^Z d_{ii'}}{k} \quad (42)$$

III. CASE STUDY

Due to the proposed integration construction of the Beijing-Tianjin-Xiong'an region, many people have started to adopt a dual-city lifestyle, residing in Beijing while working in Tianjin. This has led to a dramatic increase in travel demand between Beijing, Tianjin, and Xiong'an. According to the Beijing Transport Institute's 2022 report [1], during peak hours in September 2022, the total traffic volume between the sub-center and central urban area reached 366100 standard vehicles. Morning peak hours saw 20528 pcu/hour heading towards the central urban area and 19962 pcu/hour during evening peak hours. Additionally, the intercity railway between Beijing, Tianjin, and Hebei operates at 70%-80% occupancy on weekdays and over 95% on weekends [49]. Based on these data, it is apparent that the tremendous demand for intercity travel has led to saturation of highways and railways, with congestion on highways and difficulties in securing tickets for trains, especially on weekends. Therefore, there is an urgent need for a new, efficient mode of transportation to serve the intercity demand. These traffic flows present opportunities for UAM services, especially considering that certain eVTOL models (Table 1) have ranges exceeding the distance between any two cities in the Beijing-Tianjin-Xiong'an region, which is at most 150 km.

Therefore, the Beijing-Tianjin-Xiong'an (Hebei) region abbreviates as BTX, was chosen as the focal case. Statistical data, including longitude and latitude coordinates, population figures, tourist flow, transportation passenger flow, and congestion conditions, were gathered and processed from 30 potential demand points within the selected region. The

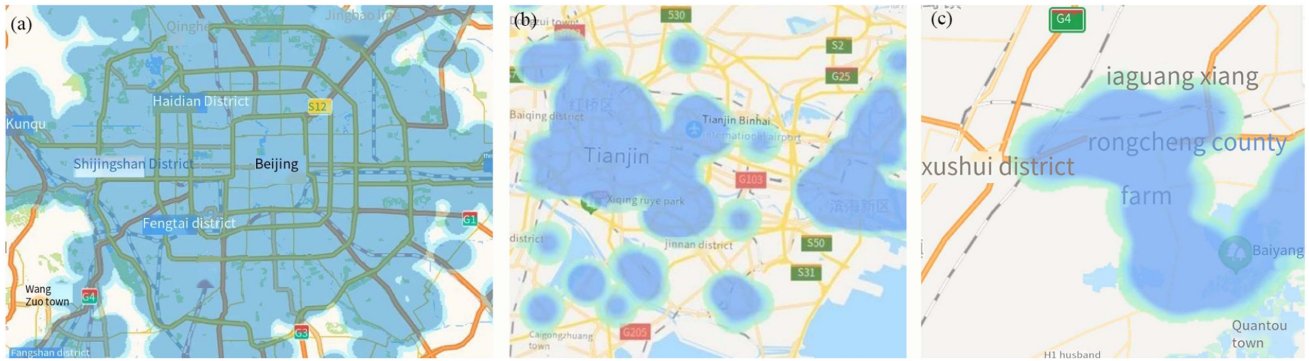


FIGURE 4. The coverage of 5G signal in Beijing (a), Tianjin (b) and Xiong'an.

algorithm and model development, simulation, and evaluation were conducted using MATLAB 2019a.

A. DATA COLLECTION AND PROCESS

The cartographic data for Beijing, Tianjin, and Xiong'an (Hebei) was sourced from DataV.GeoAtlas. The information of prohibit and restrict area were collected through Aeronautical Information Publication of China [50].

Firstly, to evaluate whether politics, size and airspace et al of the selected location meet the requirement of vertiports, the terrain within the study area was investigated and analyzed. Those areas that are dissatisfied with technical restrictions will be removed

It is worth mentioning:

- 1) Due to its vast territory, China has abundant fossil fuels and clean energy resources. In Shanxi, Inner Mongolia, and the northeastern regions of China, there are numerous coal mines used for thermal power generation. Additionally, the western regions of China, with their expansive deserts and grasslands, enjoy ample sunlight and rich wind resources, leading to the establishment of a large number of wind and solar power generation facilities. Furthermore, in the southeastern coastal cities, China has built numerous nuclear power plants, which can produce mass of electricity annually. Moreover, China's power transmission system is sufficient to deliver the electricity generated in various regions to all parts of the country. Therefore, power that the grid in any area of BTX can provide far exceeding it requires to charge a single eVTOL [34] (200-600 kW). Thus, the grid capacity constraint was not considered in our case study. Besides, due to the confidential nature of the electrical grid data for specific districts and counties, this paper does not provide a detailed discussion here. However, for countries without enough grid capacity, this should be carefully evaluated
- 2) Moreover, with the development of 5G/6G technology and its characteristic of high transmission speed, high data security, low latency and high concurrency which are critical characteristic for supporting real time UAM

communication, using 5G/6G technology as a communication means between eVTOLs is an inevitable trend for the future development of urban air traffic, in China [50]. Owing to the full coverage of 5G signals in the Beijing-Tianjin-Xiong'an urban regions, CNS constraints in urban area were not considered as well (Fig. 4). However, this could contribute to the vertiports mainly gathered in urban areas.

- 3) As the railways, cloverleaf interchanges, airports always locate far from residential buildings citizens live and could produce higher noise compared with eVTOL. Therefore, if the vertiports are selected close to these facilities, the noise and privacy concerns it brings to the citizens could be neglected in this article [24].

These assumptions will result in the majority of vertiport positions being located in the urban areas of BTX—owing to the coverage of 5G—near the noisy facilities such as railways, cloverleaf interchanges, airports. The advantage of this strategic placement is that the noise of eVTOL will be masked to the greatest extent and will better serve the travel demand in urban area. However, there are also limitations brought by these assumptions: The vertiports selected under these assumptions may not serve suburban demand better. Although the travel demand in suburban is lower than urban, this will cause the inequality between urban and suburban. Besides, for cities that have not achieved 5G coverage or have limited grid capacity, these assumptions will need carefully consideration.

Besides, to ensure the availability to operate, the climate condition including visibility and wind scale from April 2023 to April 2024 have also been collected. The fluctuate curve of congestion coefficient, noise, passenger flow, visibility, wind force in BTX are illustrated in Figs. 5 and 6. Herein, as congestion coefficient and environment noise L_{en} vary with the location and hours, which is a huge dataset, thus part of these curves is displaced in Fig. 6. Moreover, to evaluate the noise constraints, noise of these vertiports have been calculated based on (3). The noise produced by eVTOL L_{max} is 62 dB when d_1 equals to 76 m according to the research of Bain J [52]. The final maps that are suitable for the construction of vertiports are illustrated in Fig. 7.

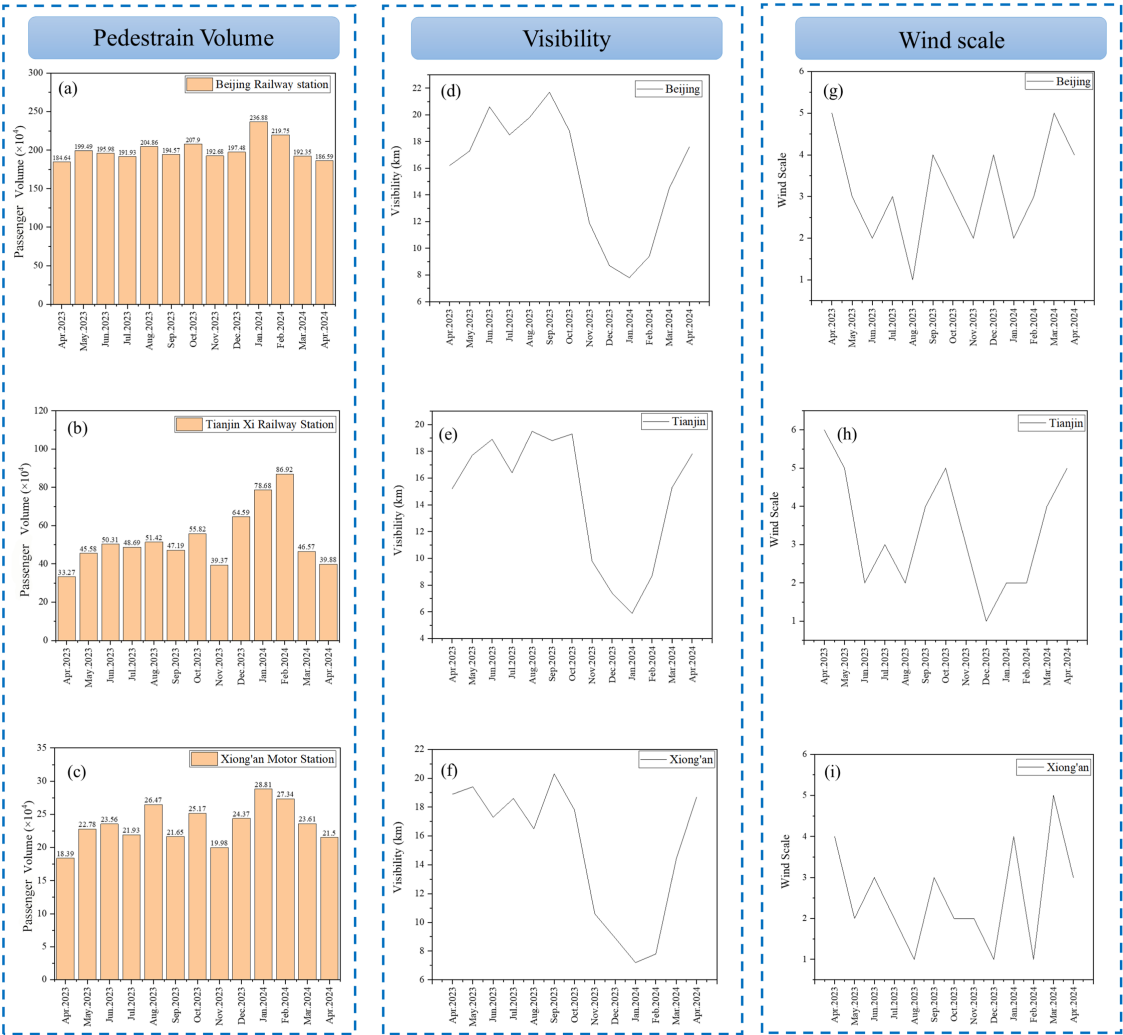


FIGURE 5. The passenger volumes (a)-(c), Visibility (d)-(f), Wind scale (g)-(i) in Beijing-Tianjin-Xiong'an.

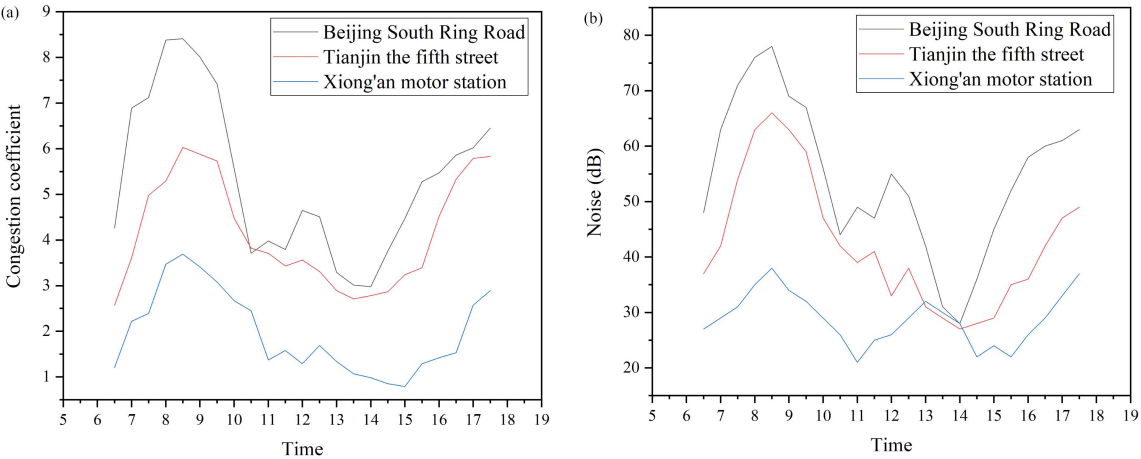


FIGURE 6. The fluctuate curve of Congestion Coefficient (a) and Noise (b) over time in Beijing South Ring Road (black); Tianjin Fifth street (red) and Xiong'an motor station (blue) in June 21, 2023.

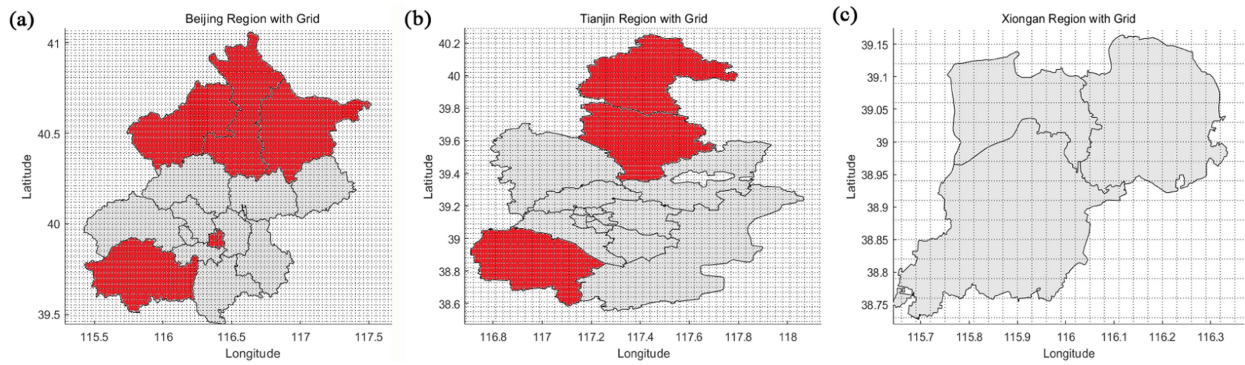


FIGURE 7. Area that dissatisfy (in red) with technical constraints in BTX (a) Beijing; (b) Tianjin; (c) Xiong'an.

It can be observed from Fig. 7 that some districts (in red) in Beijing and Tianjin do not meet the technical requirements while all the districts in Xiong'an satisfy. For Beijing, area within The Third Ring Road is prohibit area, what's more, the west and north districts of Beijing are situated on mountains. Therefore, these areas cannot be selected as vertiport candidate sites. As for Tianjin, the north of Tianjin also locates near mountains and thus is removed. Besides, as the south-west of Tianjin is suburban area which has not yet achieved 5G coverage and is removed as well. However, owing to the small size of Xiong'an and its geographic location, which is situated on North China Plain. It is not hard to achieve the full coverage of 5G without considering geographic terrain.

Due to the heterogeneous distribution of population density and the concentrated presence of tourist attractions, as well as observable congestion within the Central Business District (CBD), our study focused its data collection efforts within a circular area with a radius of 5 km centered on the designated demand point. As a result, the investigation area, as outlined in (2), encompasses an area of 78.54 km². Statistical data within this area was obtained from municipal authorities and the Shuwei platform, while terrain characteristics and congestion coefficients were acquired from Amap. The multi-dimensional input parameter related in this article was demonstrated in Table 7.

As the flight rule for UAM is mainly Visual Flight Rule (VFR) which result in the fact that eVTOLs cannot operate during evening or midnight owing to its low visibility. Therefore, in this research, all the parameters related with time are investigated within 6:30 a.m. to 17:30 p.m. each day.

After these data has been processed based on (12)–(23) and Table 7, the thermodynamic chart could be obtained. The resultant dataset is presented in Figs. 8 and 9. Figs. 8 and 9 illustrates that various types of demands within the BTX region are predominantly concentrated within the Central Business District (CBD), attributed to its dense population and employment opportunities annually. Furthermore, the suburban locations of airports in Beijing and Tianjin contribute to notable transportation demand in these areas.

TABLE 7. Input Parameters of Multi-Dimension

Dimension	Name	Value		Unit
		max	min	
Time	Operating time period	17:30	6:30	—
	Tourist volume in POI	830,000	20,000	count
	Passenger volume of airport	198,300	70,000	count
	Passenger volume of metro station	250,000	38,000	count
	Passenger volume of railway station	200,000	30,707	count
	Longitude of demand points	117.7	115.9	°
	Latitude of demand points	40.14	38.96	°
Spatial	Airspace structure	—	—	—
	Available space	43,500	4,200	m ²
	Obstacles height	597	18	m
	GDP	1102	20	billion CNY
	Population	2,138,570	98,721	count
	Commuting demand	1,283,142	59,232	count
	Tourism demand	784,000	0	count
Spatial-temporal	Noise	70	20	dB
	Visibility	10,700	1,700	m
	Wind force	5	0	—
	Congestion coefficient	8.10	1.61	—

B. VERTIPORTS LOCATION SELECTION

1) FILTER THE POTENTIAL DEMAND POINTS

To evaluate the demand of different potential demand points, the total demand density (D_i) was estimated based on (24). Due to the high volume of commuters and the importance to construct the comprehensive transport network, the values assigned to γ_{Cd} and γ_T are the highest both equaling to 0.3. As not all residents living in this region have the demand to travel far from their home and only during specific periods

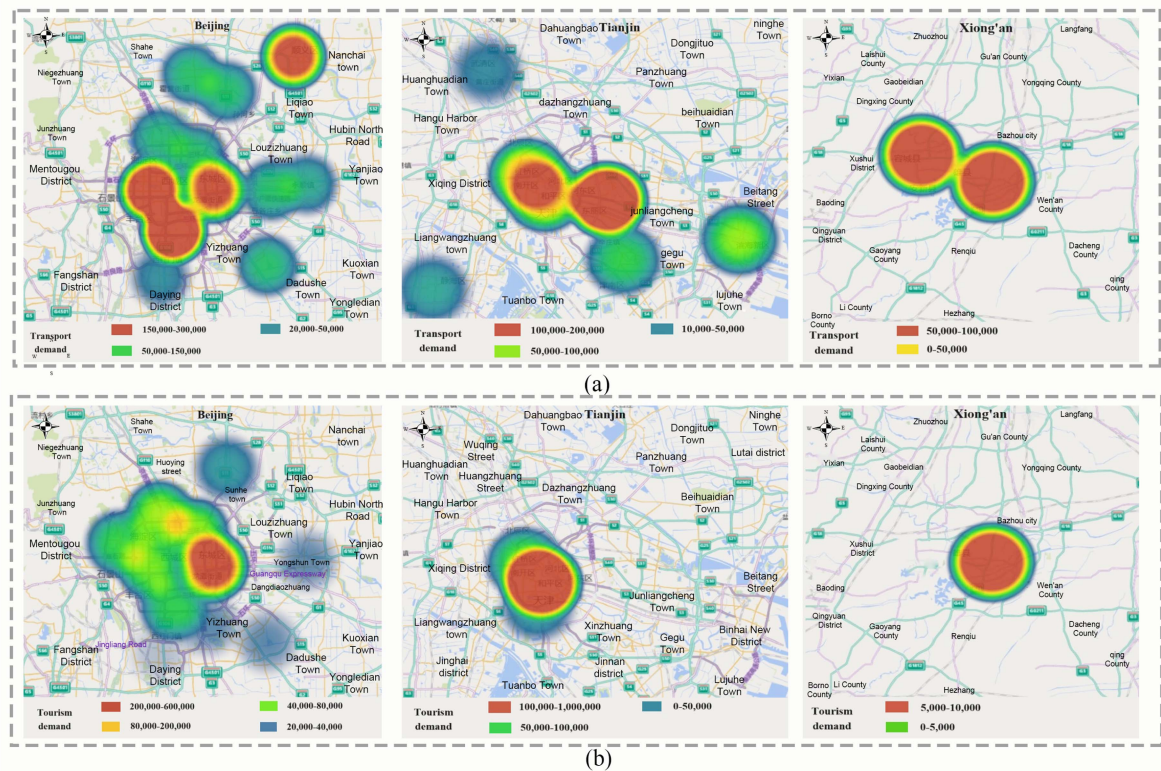


FIGURE 8. Thermodynamic chart of BTX (a) Transport demand distribution; (b) Tourism demand distribution.

TABLE 8. Total Demand Density of Different Potential Demand Points

Potential demand point	Total demand density (D_i)	Potential demand point	Total demand density (D_i)
P1	8,632.86	P12	1,957.28
P2	4,764.43	P13	1,031.14
P3	5,411.36	P14	1,530.93
P4	2,432.12	P15	1,580.15
P5	5,653.18	P16	7,555.36
P6	3,958.69	P17	1,421.85
P7	1,509.09	P18	4,857.94
P8	2,006.98	P19	2,936.36
P9	1,049.58	P20	2,525.99
P10	1,554.15	P21	1,027.70
P11	1,948.37		

of the year does tourism demand proliferate, the weight of population (γ_P) and tourism demand (γ_{Td}) is the lowest which is 0.1. The equation leveraged to compute demand density is as follows.

$$D_i = \frac{(P_i \times 0.1 + T_i \times 0.3 + T d_i \times 0.1 + C d_i \times 0.3 + A t_i \times 0.2)}{78.54} \quad (43)$$

The cumulative demand density is delineated in Table 8. Demand points characterized by a density of less than 1000 ($D_i \leq 1000$) are deemed insufficient and have been excluded from subsequent analysis. The positions of both excluded (highlighted in red) and retained (highlighted in green) demand points are visualized in Fig. 10. As depicted in

Fig. 10, demand exhibits a propensity to cluster in economically developed and densely populated areas, such as urban centers or Central Business Districts (CBDs), aligning with empirical observations.

2) VERTIPOINT LOCATION OF BTX

The data collected from April 2023 to March 2024 in BTX was utilized as input to identify the location of vertiports in BTX case study. To identify the optimal number of clusters (k), the elbow method was employed. The results of this method are presented in Fig. 11, which illustrates the curve depicting the relationship between the number of clusters and the sum of squared errors (SSE). From Fig. 11, it is apparent that the SSE value stabilizes after $k=6$, indicating that additional clusters do not significantly improve the clustering quality. Therefore, based on the elbow method, the optimal number of vertiports (k) is determined to be 6. Subsequently, considering the spatial distribution of demand points and the determined number of vertiports, a refined K-means algorithm has been utilized to identify vertiport locations. Specifically, three vertiports were identified in Beijing, two in Tianjin, and one in Xiong'an, as illustrated in Fig. 12. The variation in the number of vertical takeoff and landing points across different regions can be attributed to disparities in economic development levels, with Beijing exhibiting the highest level, followed by Tianjin, and finally Xiong'an.

The longitude and latitude coordinates of these vertiports are demonstrated in Table 9. The location of these vertiports

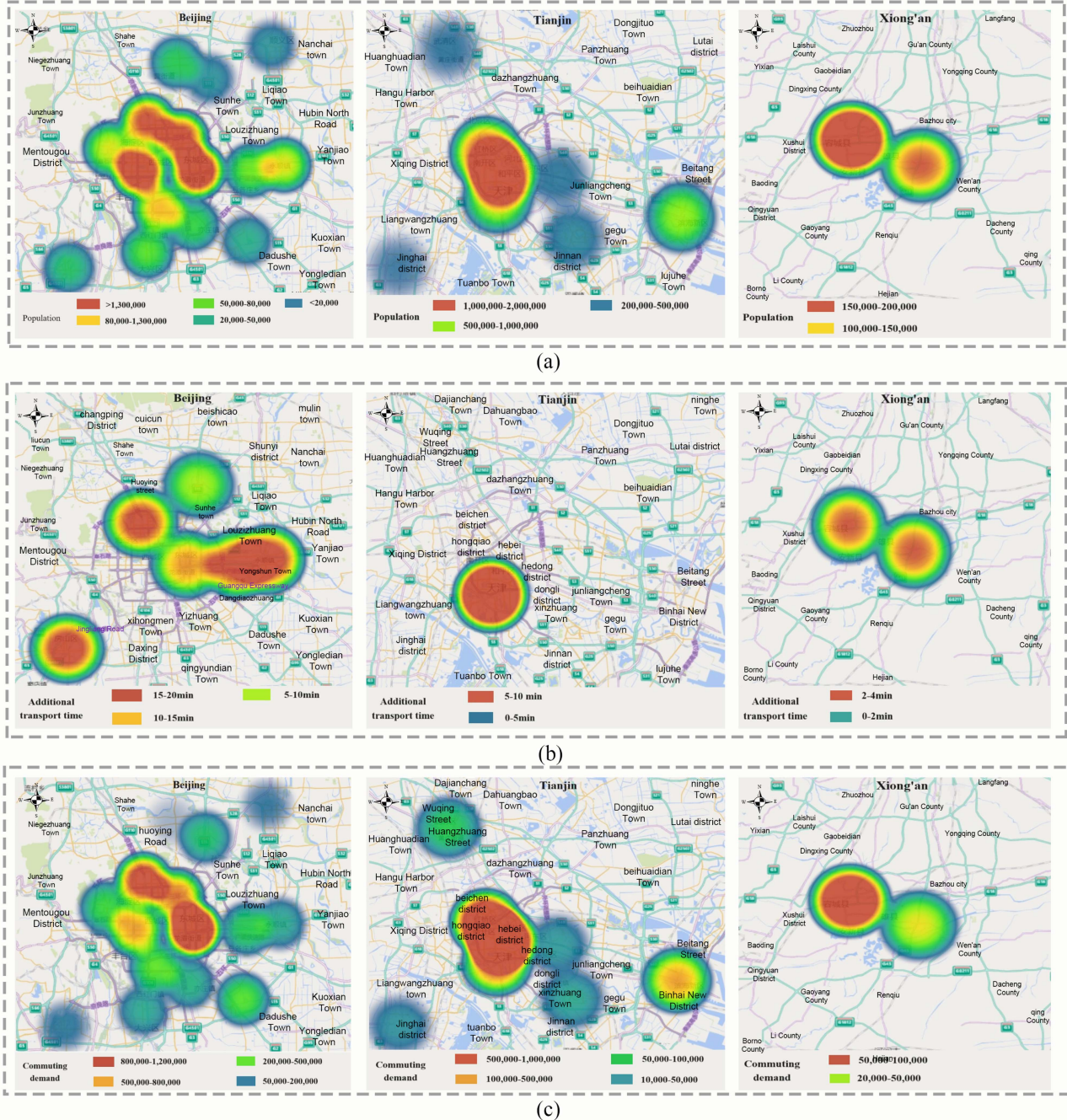


FIGURE 9. Thermodynamic chart of BTX (a) population distribution; (b) additional transport time distribution; (c) commuting demand.

TABLE 9. The Lon-Lat Coordinates of Vertiports

Location	Longitude and latitude coordinates
A	117.50,39.04
B	117.20,39.18
C	116.20,39.84
D	116.40,39.86
E	116.62,40.04
F	116.10,39.01

in Table 9 were abbreviated as alphabet A to F and were illustrated in appendix correspondingly. The relative position between the vertiports and the demand points are shown in Fig. 13.

3) VERTIPORT LOCATION OF VALIDATION CASE STUDIES TAKING BEIJING AS AN EXAMPLE

To evaluate the scalability of the proposed method, the model proposed above was further applied to case study in Beijing,

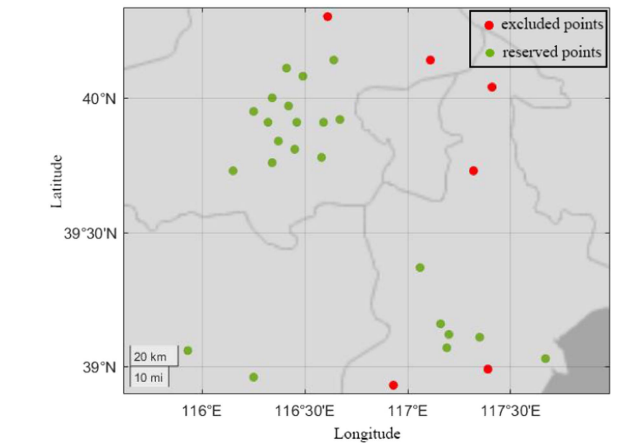


FIGURE 10. The location of excluded (red) and reserved (green) demand points.

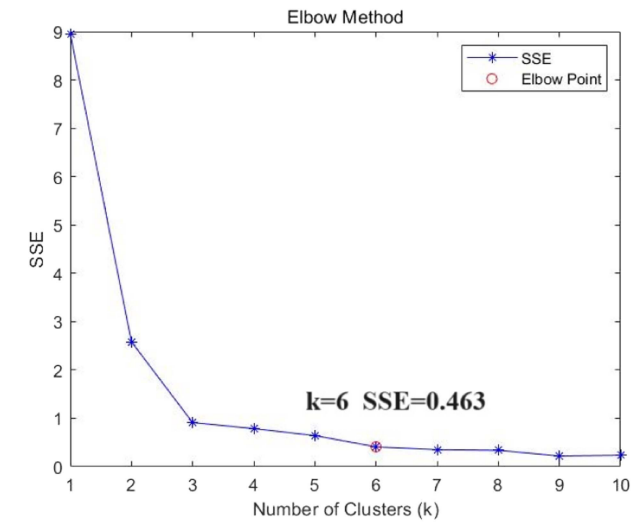


FIGURE 11. The result curve of elbow method in BTX case study.

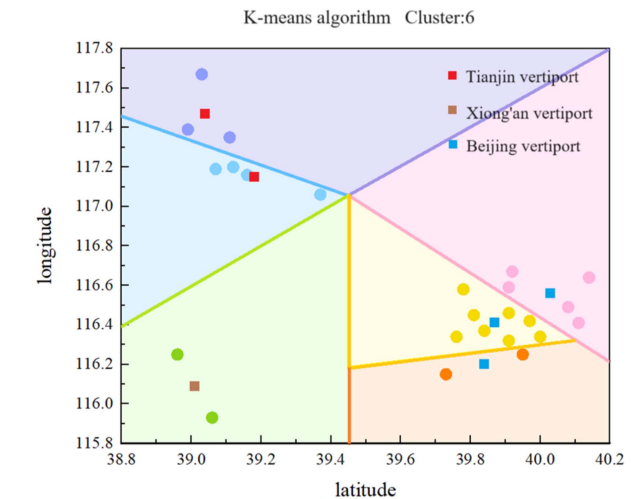


FIGURE 12. The location of vertiports obtained from K-means algorithm.

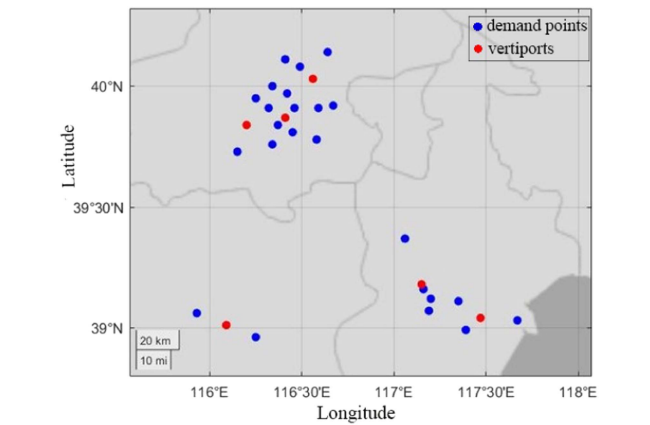


FIGURE 13. Vertiports and demand points location across BTX.

TABLE 10. The Vertiport Location and Distance Deviation in Beijing Case Study

Vertiport location	Deviation distance(km)	Average deviation distance e (km)
(116.2,39.86)	4.5	5.3
(116.5,40.11)	6.7	
(116.4,39.86)	2.1	
(116.2,39.74)	5.8	
(116.5,40.09)	6.2	
(116.6,39.91)	5.4	
(116.6,39.78)	6.3	

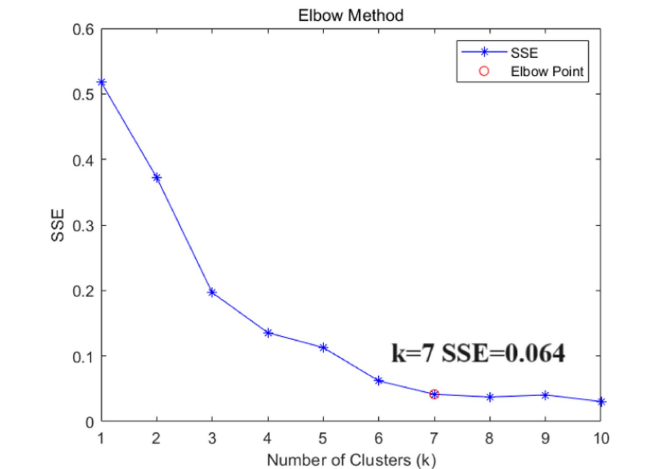


FIGURE 14. The result curve of elbow method in Beijing case study.

based on data collected in April 2024, which has been selected as validation study with distance deviation as error. The results of Beijing were given in Table 10 and Figs. 14-15. All the distance deviation of different validation case studies are lower than 8 km and the average distance deviation e is 5.3 km.

It is obvious from Fig. 14 that the value of SSE remains constant after $k=7$, indicating that additional clusters do not significantly improve the clustering quality. Thus, the amount of vertiport in Beijing case study was set as 7. The location

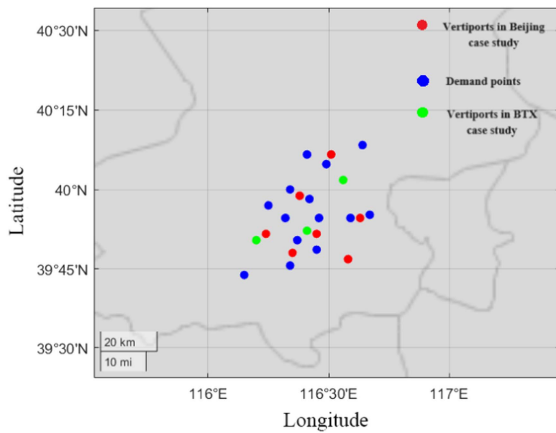


FIGURE 15. The comparison of vertiports location between BTX and Beijing case study.

TABLE 11. The Area Vertiports Locate and Height Around

Vertiport location	The area it locates(m ²)	Highest height within 100 m(m)
A	40,000	36
B	12,000	21
C	22,700	21
D	4,200	30
E	43,500	18
F	22,000	20

of these 7 vertiports in Beijing case study was displaced in Fig. 15. The reason for having more vertiports in Beijing case study compared to BTX is because when the selection area is narrowed, the distribution of demand points become more dispersed. However, even the case study area was narrowed, the selected locations remained largely unchanged with a maximum deviation distance 6.7 km as Table 10 illustrates, thus the scalability of the proposed model was confirmed. According to the computational time evaluation method given by C. Zhu [46] et al, the computational time of the proposed algorithm is 3.1 min for Beijing case study and 28.7 min for BTX case study.

C. EVALUATION OF VERTIPORTS LOCATION

1) TECHNICAL ANALYSIS

The vertiports' surrounding terrain and their walking time to transport stations nearby are shown in Fig. 16. It can be observed from Fig. 16 that all the time it takes to walk from ground transportation station to the vertiport is less than or equal to 10 min such as from Beijing Third Ring South Middle Road to Bus station 120—8 min; from Xiong'an motor station to Bus station 106—4 min; from Tianjin freeway construction center to metro line 3—9 min; from Tianjin YH park to bus station 126—10 min

The size of available space at the location of the takeoff and landing sites and the height of obstacles within 100 m were illustrated in Table 11 and Fig. 16. It can be told from Table 11

TABLE 12. Noise (dB) Level of Different Distance Around Vertiports

Vertiports	Noise of 200 m (dB)	Noise of 400 m (dB)	Noise of 600 m (dB)	Noise of 800 m (dB)
A	54	48	45	43
B	72	64	70	66
C	54	52	53	50
D	74	72	75	73
E	75	73	74	71
F	73	75	75	71

that all the selected areas could accommodate a vertical take-off and landing station with at least 4 pads which is 3600 km² in total. Fig. 16 illustrates the uneven distribution of obstacle heights within a 100 m radius around the vertiports. However, it is noteworthy that even the tallest obstacle, a department around Tianjin YH park, measuring 36 m in height, does not surpass the height limitation of 43 m, taking into account the elevation of the vertiports [10], [13], [20], [21]. The height of the rest of the obstacles around other vertiports have also been demonstrated in Table 11.

The noise estimated nears the vertiports have been displaced in Table 12. It can be observed from Table 12 that all the noise falls below 75 dB, which equals to the noise produced by busy center street. This can be attributed to the fact that the vertiports (B,D,E,F) in this study are strategically positioned near railways, clover-leaf interchanges, airports or motor stations as Fig. 16 illustrates. This strategic placement may ensure the privacy of citizens [24] and potentially obscure most of the noise generated by eVTOL operations with the noise produced by trains, cars, or airplanes especially during peak hours [24], which could produce noise between 70-80 dB as it is demonstrated in Fig. 6. Besides, it can be observed that the noise in vertiport A and C are much lower than others. This can be attributed to the fact that these vertiports are located far from the noisy facilities mentioned above and thus the noise produced by eVTOL has not been totally obscured. Although the noise from eVTOL at vertiports A and C are not fully masked due to the park setting and lower traffic level, the noise level remains below 60 dB, meeting the national noise emission standards published by China [33]

Moreover, it can be concluded that all the vertiports have been selected between the Third and Fifth Ring Road of Beijing, in the urban of Tianjin and Xiong'an. Namely, none of them have been selected in the prohibited airspace which is within the second ring of Beijing, making it possible for the operation of eVTOL.

The criterion for eVTOL to take-off and landing was obtained referring to the standard published by CAAC [53], [54], [55], with its visibility at least 1600 m and the wind force should not exceed 8 Beaufort scale. As Fig. 5 illustrates, the annual minimum visibility in BTX is at least 6000 m with a maximum wind force of 6 on the Beaufort scale, meeting the minimum flight standards, thus allowing for the establishment of vertiport in BTX. Besides, the days that exceed the eVTOL criterion to take-off and landing in BTX has been displaced in Table 13.

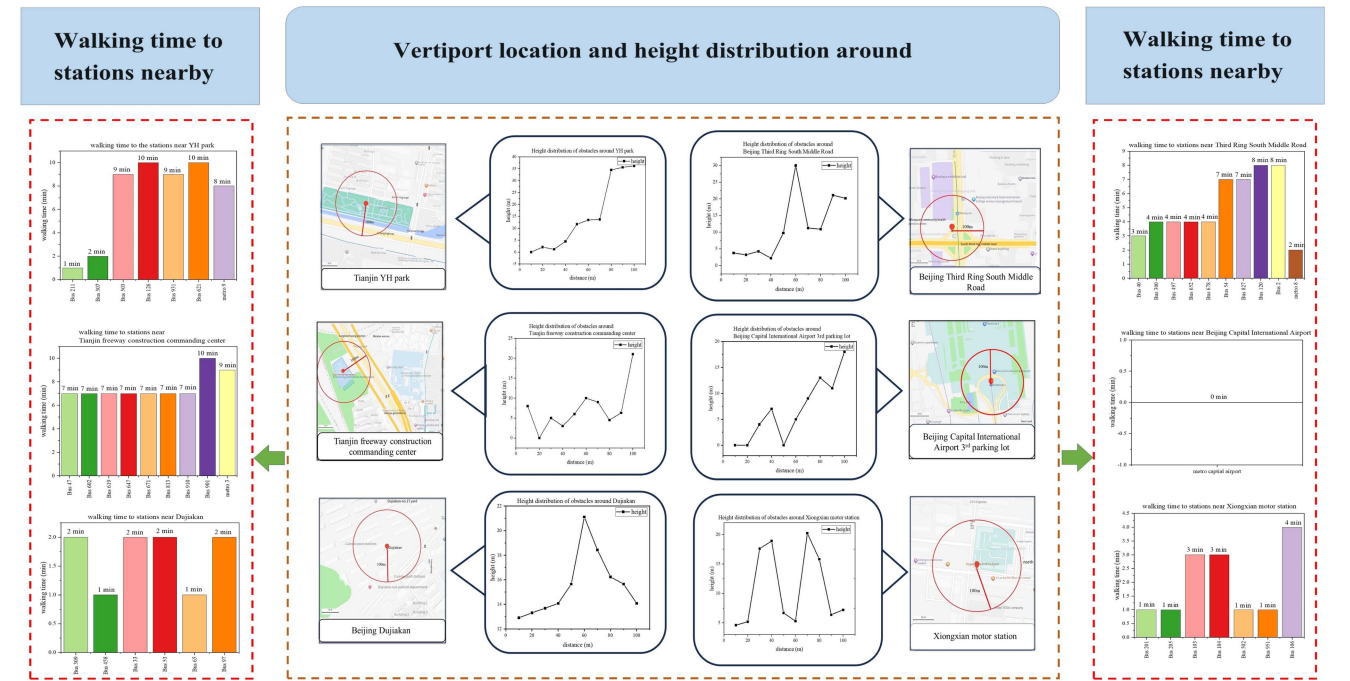


FIGURE 16. The surrounding terrain of vertiports.

TABLE 13. The Days That Dissatisfied With the Takeoff and Landing Criterion Within a Year

Region	Days that exceed the criterion
Beijing	36
Tianjin	42
Xiong'an	27

TABLE 14. Distance (km) Between Different Vertiports

	A	B	C	D	E	F
A	0	30.20	142.74	132.05	134.44	120.98
B	30.20	0	112.89	102.93	107.59	96.79
C	142.74	112.89	0	17.39	40.12	92.69
D	132.05	102.93	17.39	0	24.64	99.04
E	134.44	107.59	40.12	24.64	0	121.26
F	120.98	96.79	92.69	99.04	121.26	0

Furthermore, Table 13 indicates that the number of days not meeting the eVTOL takeoff and landing criteria in any region is less than 2 months, which also ensures the normal operation of eVTOLs

2) DEMAND AND ECONOMIC ANALYSIS

Tables 14 and 15 illustrate the distance and ticket price between vertiports. It can be concluded that the ticket price between two vertiports is directly proportional to its distance.

Based on these data and (40), the number of passengers served between vertiports were calculated and presented in Table 16. The total amount of passengers served by each

TABLE 15. Ticket Price (CNY) Between Different Vertiports

	A	B	C	D	E	F
A	0	141.98	149.34	148.64	148.79	147.91
B	141.98	0	147.38	146.73	147.04	146.33
C	149.34	147.38	0	141.14	142.62	146.06
D	148.64	146.73	141.14	0	141.61	146.48
E	148.79	147.04	142.62	141.61	0	147.93
F	147.91	146.33	146.06	146.48	147.93	0

TABLE 16. Service Passenger Between Vertiports

	A	B	C	D	E	F
A	0	3,039	3,704	3,576	1,402	800
B	3,039	0	4,164	4,038	3,419	1,949
C	3,704	4,164	0	16,843	10,796	4,329
D	3,576	4,038	16,843	0	12,012	3,947
E	1,402	3,419	10,796	12,012	0	1,439
F	800	1,949	4,329	3,947	1,439	0

pair of vertiports in Table 16 is 75465 passengers and could effectively relieve the ground transportation pressure.

Furthermore, to enhance connectivity between various modes of transportation and facilitate seamless inter-city or intra-city travel for passengers, all vertiports were strategically positioned adjacent to transportation hubs such as metro stations, airports, bus stations, or motor stations, as depicted in Fig. 16. Each vertiport is equipped with at least one mode of transportation to accommodate disembarking passengers,

TABLE 17. The Lon-Lat Coordinates of Vertiports Obtained From So.J [26] Model

Location	Lon-lat coordinates
(a)	(116.44,39.88)
(b)	(116.34,40.00)
(c)	(116.47,40.01)
(d)	(117.21,39.13)
(e)	(117.20,39.05)
(f)	(116.11,39.00)

and the maximum walking time required to reach these transportation stations from the vertiports is limited to 10 min. This strategic placement not only facilitates convenient transfers between different modes of transportation but also helps alleviate pressure on ground transportation systems.

In conclusion, the site selection process for eVTOL deployment across the Beijing-Tianjin-Xiong'an (Hebei) region considered a range of influential factors, including population density, commuting patterns, regional economic vitality, tourism dynamics, traffic congestion levels, and specific requirements for Vertical Takeoff and Landing Airports. Leveraging collected statistical data, six optimal vertiport locations were determined using the *K*-means.

To evaluate the viability of the chosen sites for vertiport establishment, comprehensive assessments were conducted, encompassing geographical considerations, minimum area prerequisites, and obstacle height constraints. As a result, all vertiport sites were found to meet the necessary criteria effectively.

Moreover, a demand forecasting model was employed to assess the potential impact of eVTOL implementation under this vertiport configuration. The outcomes of the gravity model indicated that the collective capacity of the vertiport network could accommodate up to 75645 passengers, thus substantially alleviating the strain on ground transportation systems.

The result of this study could provide reference suggestions for the selection problem of vertiports location considering technical regulations such as terrain, noise et al in the future. Besides, it may also offer reference for the future constructions of vertiports and the basic requirements for its necessary infrastructures such as CNS facilities and charging pole. Lastly, the economic evaluation in this study might supply an overview of the future UAM market for future eVTOL service providers.

3) COMPARE AND CONTRAST

To further illustrate the effectiveness of this proposed method, model proposed by J. So et al [26], which takes relatively comprehensive factors such as demand, obstacle height, location of transportation hubs, noise and privacy according to Table 3, has also been utilized in this BTX case study. The demand was also calculated utilizing (46). The results are illustrated in Fig. 17. The lon-lat coordinates have been displaced in Table 17.

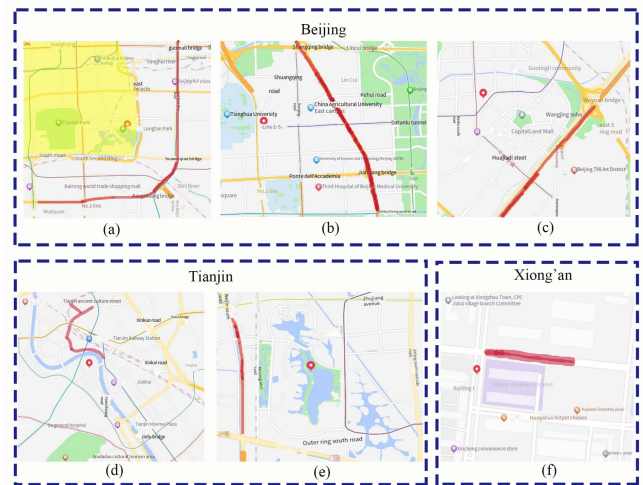


FIGURE 17. The airspace and congestion condition of vertiports obtained using model developed by J. So [26].

TABLE 18. The Congestion Condition Around Vertiports Selected Using Different Method in Different Cities

Research	Location	Average Congestion Coefficient
J. So [26]	Beijing	4.36
	Tianjin	3.58
	Xiong'an	2.01
The proposed method	Beijing	5.29
	Tianjin	3.67
	Xiong'an	2.02

The prohibited airspace has been marked in yellow and the roads that have a high congestion condition have been marked in red. It can be concluded from Fig. 17 that the vertiports location obtained using J. So et al [26] method have at least one highly congested road section around which satisfied the congestion constraint. However, owing to the low importance index in J. So [26] study, the average congestion coefficient of roads covered by these vertiports in different cities are lower than it is in this study according to Table 18 and thus may impair the degree of alleviating ground transportation pressure.

Moreover, as it can be observed from Fig. 17 that vertiport (a) locates within the prohibit zone in the airspace. This could be attributed to the overlook of airspace structure and may lead eVTOL to be unable to takeoff.

Besides, it can also be told from Fig. 18 that all these vertiports obtained through J. So [26] have either a metro station, motor station or railway station around which proves the enough transfer opportunity and could serve the transportation demand. However, as the model used in J. So [26] study deems transfer opportunity more important than the transfer convenience. Therefore, it can be concluded from Fig. 18 and Table 19 that the average walking distance from vertiport to these transportation hubs are 87 m ~2.79 km and will take 1~27 min to walk. However, as it has been mentioned in Fig. 18, the walking time from these vertiports obtained in our study to transportation hubs is no more than 10 min, which significantly increase the transfer convenience.

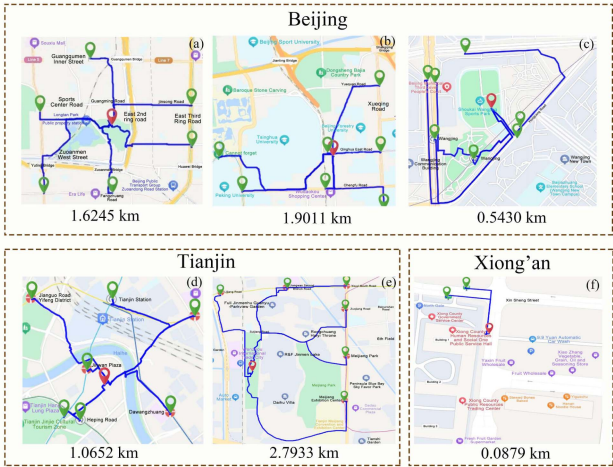


FIGURE 18. The walking distance from transportation hubs (green labels) to vertiports (red labels) obtained using model developed by J. So [26].

TABLE 19. The Transfer Convenience and Potential Tourism Demand of Two Studies

Research	Location	Average walking distance (km)	Average walking time (min)	Tourism demand (count)
J. So [26]	(a)	1.6245	15	2,974,725
	(b)	1.9011	18	
	(c)	0.5430	6	
	(d)	1.0652	10	
	(e)	2.7933	27	
	(f)	0.0879	1	
The proposed method	A	0.5884	7	3,683,100
	B	0.6721	8	
	C	0.1686	2	
	D	0.4239	5	
	E	0	0	
	F	0.1682	2	

Moreover, as tourism demand has not been considered in the research conducted by J. So [26], the potential tourist demand that could be served by eVTOL is lower than it is in this study and may further reduce the revenue especially during holiday.

IV. CONCLUSION

The paper presents a comprehensive investigation into the site selection and evaluation model for the deployment of electric Vertical Take-off and Landing (eVTOL) aircraft. Technical factors influencing site selection, including airspace, CNS constraints, grid capacity, terrain, climate, noise and demand, are thoroughly analyzed to identify the optimal vertiport locations. The suitability of these vertiport locations is rigorously assessed based on technical factors. All the vertiport sites obtained in this article have no intersection with the prohibited or restricted airspace. Besides, the location of these sites obtained in this case study satisfied the obstacle restrictions, which is 43 m, and could accommodate a vertiport with at least 4 pads and is suitable for eVTOL to take-off and landing.

TABLE 20. The Location of Vertiports and Their Corresponding Abbreviations

Location	Abbreviation
Tianjin YH park	A
Tianjin freeway construction commanding center	B
Beijing Dujiakan	C
Beijing Third Ring South Middle Road	D
Beijing Capital International Airport 3 rd parking lot	E
Xiongxian motor station	F

TABLE 21. GDP of Different District in Beijing-Tianjin-Xiong'an

District	GDP (billion yuan)	District	GDP (billion yuan)	District	GDP (billion yuan)
Haidian (Beijing)	1102	Fangshan (Beijing)	88	Dongli (Tianjin)	72
Chaoyang (Beijing)	839	Huairou (Beijing)	48	Heping (Tianjin)	67
Xicheng (Beijing)	600	Pinggu (Beijing)	45	Jinghai (Tianjin)	50
Dongcheng (Beijing)	357	Miyun (Beijing)	37	Hedong (Tianjin)	49
Shunyi (Beijing)	220	Yanqing (Beijing)	22	Baodi (Tianjin)	42
Fengtai (Beijing)	219	Hexi (Tianjin)	115	Hebei (Tianjin)	38
Changping (Beijing)	142	Xiqing (Tianjin)	100	Ninghe (Tianjin)	32
Tongzhou (Beijing)	130	Wuqing (Tianjin)	96	Jizhou (Tianjin)	29
Shijingshan (Beijing)	107	Nankai (Tianjin)	75	Hongqiao (Tianjin)	20
Daxing (Beijing)	104	Beichen (Tianjin)	74	Xiong'an (Xiong'an)	41

The visibility within the selected area is at least 6000 m and Beaufort scale is at most 6 which meet the safety constraints for eVTOL to take-off and landing. As most of the vertiports are displaced around the railways, clover-leaf interchanges, or airports, which could produce noise between 70-80 dB, the noise generated by the operation of eVTOL could be largely concealed by the noise of car, train and airplane. Moreover, a demand forecasting model is utilized to evaluate the potential impact of eVTOL deployment on passenger transportation, revealing a notable alleviation of pressure on ground transportation systems, which is 75465 passengers in count, as demonstrated in a case study. Moving forward, future research will focus on flight route and schedule design based on the identified take-off and landing points, aiming to enhance the overall operational efficiency of eVTOL transportation systems.

APPENDIX

Table 20 gives the location of vertiports and their corresponding abbreviations. Table 21 gives GDP of different districts in Beijing-Tianjin-Xiong'an. Table 22 shows original data used in the study, and Table 23 shows the processed data. Table 24 shows the location of demand points.

TABLE 22. The Original Data Used in This Study

Demand Point	Population	Commuter	Tourist	Congestion coefficient
P1	1,767,300	2,138,570	830,000	4.511
P2	1,426,550	1,071,639	333,100	0
P3	1,361,883	1,389,202	345,000	5.94
P4	854,258	482,182	235,000	0
P5	1,721,075	965,851	300,000	0
P6	1,019,973	548,878	220,000	0
P7	333,157	163,378	0	0
P8	681,651	430,335	0	0
P9	524,876	99,703	0	6.192
P10	332,332	377,933	110,000	0
P11	415,090	530,646	50,000	3.668
P12	2,240,293	1,518,159	980,000	0
P13	352,087	148,132	0	0
P14	1,709,041	982,990	200,000	0
P15	1,125,094	620,617	80,000	2.401
P16	941,828	518,936	0	0
P17	340,305	243,530	0	0
P18	133,650	34,762	12,000	0
P19	870,603	298,117	50,000	0
P20	484,360	180,812	0	0
P21	568,883	329,727	50,000	6.51
P22	215,015	108,197	0	6.563
P23	196,497	98,721	30,000	0
P24	389,245	166,801	0	0
P25	290,434	109,429	20,000	0
P26	263,138	108,604	0	0
P27	322,559	136,192	0	0

TABLE 23. The Processed Data in This Study

Demand Point	Tourism Demand	Commuting Demand	Transport & Transfer demand	Additional travel time
P1	664,000	1,283,142	166,500	12
P2	266,480	642,983.4	40,000	0
P3	276,000	833,521.2	37,200	16
P4	188,000	289,309.2	0	0
P5	240,000	579,510.6	246,800	0
P6	176,000	329,326.8	308,400	0
P7	0	98,026.8	186,000	0
P8	0	64,918.2	40,000	0
P9	0	258,201	40,000	16
P10	0	59,821.8	40,000	0
P11	88,000	226,759.8	40,000	8
P12	784,000	910,895.4	59,000	0
P13	0	88,879.2	166,000	0
P14	160,000	589,794	59,000	0
P15	64,000	372,370.2	0	8
P16	0	311,361.6	36,000	0
P17	0	146,118	9,500	0
P18	9,600	20,857.2	40,000	0
P19	40,000	318,387.6	30,000	0
P20	24,000	59,232.6	0	0
P21	40,000	178,870.2	0	17
P22	0	108,487.2	0	17
P23	40,000	197,836.2	30,707	0
P24	0	100,080.6	24,400	0
P25	16,000	656,57.4	36,000	0
P26	0	65,162.4	14,000	0
P27	0	81,715.2	14,000	0

TABLE 24. The Location of Demand Points

Demand point	Lon-lat coordinates	Demand point	Lon-lat coordinates
P1	(116.46,39.91)	P15	(117.19,39.07)
P2	(116.42,39.97)	P16	(117.67,39.03)
P3	(116.34, 40.00)	P17	(117.06,39.37)
P4	(116.25,39.95)	P18	(117.39,38.99)
P5	(116.32,39.91)	P19	(116.67,39.92)
P6	(116.37,39.84)	P20	(116.15,39.73)
P7	(116.64,40.14)	P21	(116.45,39.81)
P8	(116.59,39.91)	P22	(117.10, 40.13)
P9	(116.41,40.11)	P23	(116.60, 40.29)
P10	(116.49,40.08)	P24	(117.38,38.98)
P11	(116.58,39.78)	P25	(117.40,40.03)
P12	(117.20,39.12)	P26	(117.31, 39.72)
P13	(117.35,39.11)	P27	(116.92,38.92)
P14	(117.16,39.16)	—	—

REFERENCES

- [1] Beijing Transport Institute, "Beijing transport development annual report," ed., Rep., Sep. 2022. [Online]. Available: <https://www.bjtrc.org.cn/List/index/cid/7.html>
- [2] INRIX, "Global traffic score card," ed., Rep., Jan. 2023. [Online]. Available: <https://inrix.com/scorecard/#form-download-the-full-report>
- [3] Uber Elevate, "Fast-forwarding to a future of on-demand urban air transportation," ed., Rep., Oct. 27, 2016. [Online]. Available: https://d1nyezh1ys8wfo.cloudfront.net/static/PDFs/Elevate%2BWhitepaper.pdf?uclid_id=4e6d76ac-7c01-42ea-948c-ef4839e8345d
- [4] Tianjin Government, Expansion of Wuhan Beijing Tianjin intercity trains (edition) [News]. Jun. 2023. [Online]. Available: https://www.tj.gov.cn/sy/zwdt/gqdt/202306/t20230620_6327312.html
- [5] International Energy Agency, "CO₂ emissions in 2022," IEA, Paris, France, Tech. Rep. CC BY 4.0, Mar. 2023.
- [6] Aerospace Industries Association, "Horizon 2050: A flight plan for the future of sustainable aviation," ed., Rep., Apr. 19, 2022. [Online]. Available: <https://www.aia-aerospace.org/publications/horizon-2050-new-report-from-aia-accenture-details-strategic-plan-for-the-future-of-sustainable-aviation/>
- [7] NASA, "Urban air mobility market study," ed., Res., Nov. 18, 2018. [Online]. Available: <https://ntrs.nasa.gov/api/citations/20190001472/downloads/20190001472.pdf>
- [8] FAA, "Aviation climate action plan," ed., Rep., Nov. 9, 2021. [Online]. Available: <https://www.faa.gov/sustainability/aviation-climate-action-plan>
- [9] CAAC, "Special plan for green development of civil aviation during the 14th five year plan," ed., Document, Dec. 21, 2021. [Online]. Available: <https://www.gov.cn/zhengce/zhengceku/2022-01/28/5670938/files/c22e012963ce458782eb9cb7fea7e3e3.pdf>
- [10] Europe Commission, "ReFuelEU aviation initiative," ed., Document, Apr. 2023. [Online]. Available: https://transport.ec.europa.eu/transport-modes/air/environment/refueeu-aviation_en
- [11] F. Naser, N. Peinecke, and B. I. Schuchardt, "Air taxis vs. taxicabs: A simulation study on the efficiency of UAM," in *Proc. AIAA Aviation 2021 Forum*, Jul. 2021, pp. 3202–3220.
- [12] L. E. Alvarez, J. C. Jones, and A. Bryan, "Demand and capacity modeling for advanced air mobility," in *Proc. AIAA Aviation 2021 Forum*, Jul. 2021, pp. 2381–2405.
- [13] D. N. Fadhil, *A GIS-Based Analysis for Selecting Ground Infrastructure Locations for Urban Air Mobility*. Munich, Germany: Munich Technical Univ. Press, 2018.
- [14] M. Taylor, J. Nebhard, and A. Barreal, "Design of a rapid, reliable urban mobility system for the DC region," in *Proc. 2020 Integr. Commun. Navigation Surveill. Conf.*, Herndon, VA, USA, 2020, pp. 2A1-2A1-2A1-11.
- [15] N. Venkatesh, A. P. Payan, and C. Y. Justin, "Optimal siting of sub-urban air mobility (sUAM) ground architectures using network flow formulation," in *Proc. AIAA Aviation 2020 Forum*, Jun. 2020, pp. 2921–2940.

- [16] M. Daskilewicz, B. German, and M. Warren, "Progress in vertiport placement and estimating aircraft range requirements for eVTOL daily commuting," in *Proc. 2018 Aviation Technol., Integration, Operations Conf.*, 2018, pp. 2884–2895.
- [17] X. Cheng, F. Shu, Y. Li, Z. Zhuang, D. Wu, and J. Wang, "Optimal measurement of drone swarm in RSS-based passive localization with region constraints," *IEEE Open J. Veh. Technol.*, vol. 4, pp. 1–11, 2023.
- [18] J. Jeong, M. SO, and H.-Y. Hwang, "Selection of vertiports using K-means algorithm and noise analyses for urban air mobility (UAM) in the Seoul metropolitan area," *Appl. Sci.*, vol. 11, pp. 5729–5748, Jun. 2021.
- [19] Z. Q. Wu and Y. Zhang, "Integrated network design and demand forecast for on-demand urban air mobility," *Engineering*, vol. 7, pp. 473–487, Apr. 2021.
- [20] E. Feldhoff and G. Soares Roque, "Determining infrastructure requirements for an air taxi service at cologne bonn airport," *CEAS Aeronautical J.*, vol. 12, pp. 821–833, Aug. 2021.
- [21] M. Matracia, M. A. Kishk, and M.-S. Alouini, "Coverage analysis for UAV-assisted cellular networks in rural areas," *IEEE Open J. Veh. Technol.*, vol. 2, pp. 194–206, 2021.
- [22] L. C. Willey and J. L. Salmon, "A method for urban air mobility network design using hub location and subgraph isomorphism," *Transp. Res. Part C, Emerg. Technol.*, vol. 125, May 2021, Art. no. 102997.
- [23] P. Bruesberg, A. C. Doberts, and T. M. Jansen, "Landing platform for urban air mobility vehicles integrated into parking lot infrastructure in densely built-up areas," in *Proc. 32nd Conf. Int. Council Aeronautical Sci.*, 2021, pp. 6–10.
- [24] M. Brunelli, C. C. Ditta, and M. N. Postorino, "New infrastructures for urban air mobility systems: A systematic review on vertiport location and capacity," *J. Air Transport Manage.*, vol. 112, Jul. 2023, Art. no. 102460.
- [25] K. Wang, A. Jacquillat, and V. Vaze, "Vertiport planning for urban aerial mobility: An adaptive discretization approach," *Manuf. Service Operations Manage.*, vol. 24, pp. 3215–3235, Sep. 2022.
- [26] J. So, M. Chae, and J. Hong, "Integrated mobility hub location selection for sustainable urban mobility," *Sustain. Cities Soc.*, vol. 99, Sep. 2023, Art. no. 104950.
- [27] C. Hage, T. Sophy, and E.-H. Aglzim, "Investigating UAV propellers performances near moving obstacles: CFD study, thrust control, and battery energy management," *IEEE Open J. Veh. Technol.*, vol. 4, pp. 590–609, 2023.
- [28] J. K. Ribeiro, G. M. R. Borille, and M. Caetano, "Repurposing urban air mobility infrastructure for sustainable transportation in metropolitan cities: A case study of vertiports in Sao Paulo," *Sustain. Cities Soc.*, vol. 98, Jul. 2023, Art. no. 104797.
- [29] J. K. Ribeiro and G. M. R. Borille, "GIS-based vertiport infrastructure analysis for urban air mobility operation," *Anais do XX Simpósio Brasileiro de Sensoriamento Remoto*, vol. 20, pp. 130–133, Apr. 2023.
- [30] B. Rahman, R. Bridgelall, and M. F. Habib, "Integrating urban air mobility into a public transit system: A GIS-based approach to identify candidate locations for vertiports," *Vehicles*, vol. 5, pp. 1803–1817, Dec. 2023.
- [31] CAAC, "Technical requirements of civil vertiports," ed., Document, Jun. 14, 2024. [Online]. Available: <https://www.caac.gov.cn/HDJL/YJZJ/202406/P020240617411282793136.pdf>
- [32] EASA, "Vertiports prototype technical specifications for the design of VFR vertiports for operation with manned VTOL-capable aircraft certified in the enhanced category," ed., Document, Mar. 24, 2022. [Online]. Available: <https://www.easa.europa.eu/en/document-library/general-publications/prototype-technical-design-specifications-vertiports#group-easa-downloads>
- [33] "Emission standard for industrial enterprises noise at boundary," GB 12348-2008, 2008.
- [34] S. A. Rizzi, D. L. Huff, and D. D. Boyd, "Urban air mobility noise: Current practice, gaps, and recommendations," NASA, Washington, DC, USA, Tech. Rep. NASA-TP-2020-5007433, Oct. 2020.
- [35] CAAC, "National airspace basic classification method," ed., Document, Dec. 21, 2023. [Online]. Available: <https://www.caac.gov.cn/XXGK/XXGK/TZTG/202312/P020231222621680839714.pdf>
- [36] D. P. Thipphavong, "Analysis of electrical grid capacity by interconnection for urban air mobility," in *Proc. AIAA Aviation 2022 Forum*, Jun. 2022, Art. no. 3316.
- [37] R. Gillani, J. Somia, and M. Irfan, "A proposed communication, navigation & surveillance system architecture to support urban air traffic management," in *Proc. IEEE/AIAA 40th Digit. Avionics Syst. Conf.*, 2021, pp. 1–7.
- [38] M. Cenç Ertürk, N. Hosseini, H. Jamal, A. Şahin, D. Matolak, and J. Haque, "Requirements and technologies towards Uam: Communication, navigation, and surveillance," in *Proc. IEEE 2020 Integr. Commun. Navigation Surveill. Conf.*, Herndon, VA, USA, 2020, pp. 2C2-2C1–2C2-15.
- [39] FAA, "Engineering brief no. 105, vertiport design," ed., Document, Sep. 22, 2022. [Online]. Available: <https://www.faa.gov/sites/faa.gov/files/eb-105-vertiports.pdf>
- [40] G. Gutiérrez-Jarpa, C. Obreque, and G. Laporte, "Rapid transit network design for optimal cost and origin–destination demand capture," *Comput. Operations Res.*, vol. 40, pp. 3000–3009, Jul. 2013.
- [41] G. Gutiérrez-Jarpa, G. Laporte, and V. Marianov, "Corridor-based metro network design with travel flow capture," *Comput. Operations Res.*, vol. 89, pp. 58–67, 2018.
- [42] G. Laporte, J. A. Mesa, and F. A. Ortega, "Maximizing trip coverage in the location of a single rapid transit alignment," *Ann. Operations Res.*, vol. 136, pp. 49–63, 2005.
- [43] "Road traffic information service—Traffic condition description," GB/T 29107-2012, 2012. [Online]. Available: <https://openstd.samr.gov.cn/bzgk/gb/newGbInfo?hcno=CDEC8DD188BB3129933203A85E7BBA69>
- [44] "Urban road traffic performance index," DB11/T 785-2011, 2011. [Online]. Available: <http://bz.h.scjg.beijing.gov.cn/bzh/apifile/file/2021/20210325/8660bad6-283d-44f7-9214-ff4e4f10a1cb.PDF>
- [45] L. Cilio and O. Babacan, "Allocation optimisation of rapid charging stations in large urban areas to support fully electric taxi fleets," *Appl. Energy*, vol. 295, 2021, Art. no. 117072.
- [46] C. Zhu and D. Gao, "Multiple matrix learning machine with five aspects of pattern information," *Knowl.-Based Syst.*, vol. 83, pp. 13–31, 2015.
- [47] K. Becker, I. Terekhov, and V. Gollnick, "A global gravity model for air passenger demand between city pairs and future interurban air mobility markets identification," in *Proc. 2018 Aviation Technol., Integration, Operations Conf.*, 2018, pp. 2885–2896.
- [48] I. Terekhov, *Forecasting Air Passenger Demand Between Settlements Worldwide Based on Socio-Economical Scenarios*. Hamburg, Germany: Hamburg Univ. of Tech. Press, 2017.
- [49] Tianjin Government, *140000 passengers boarding and disembarking at Tianjin Station* (edition) [News], Jan. 2011. [Online]. Available: https://www.tj.gov.cn/sy/zwdt/bmdt/202005/t20200520_2427836.html
- [50] Aeronautical Information Publication of China, CAAC, Beijing area chart, ed., News, Aug. 2019. [Online]. Available: <https://aip.chinaflir.com/#/>
- [51] F. Naeem, V. Gollnick, and C. Schmitt, "5G-enabled architectural imperatives and guidance for urban air mobility: Enhancing communication, navigation, and surveillance," in *Proc. AIAA Aviation Forum Ascend 2024*, Aug. 2024, Art. no. 3783.
- [52] J. Bain, G. Goetchius, and D. Josephson, "Fly over noise comparison between joby aircraft and similar aircraft," in *Proc. Vertical Flight Soc. 78th Annu. Forum*, May 2022, pp. 1–8. [Online]. Available: <https://www.semanticscholar.org/paper/Flyover-Noise-Comparison-Between-Joby-Aircraft-and-Bain-Goetchius/acf259259919f4b255c4dac786747daecf957f8e>
- [53] "General operating and flight rules," CCAR-91-R1, 2007. [Online]. Available: <https://www.caac.gov.cn/XXGK/XXGK/MHGZ/201511/P020151103349952434278.pdf>
- [54] "Requirements for safe operation of regular passenger flights for small aircraft and transport helicopters," AC-135-FS-002, 2023. [Online]. Available: <https://www.caac.gov.cn/XXGK/XXGK/GFXWJ/202304/P020230421372460192139.pdf>
- [55] "Regulations on the formulation and implementation of minimum standards for aircraft airport operations," CCAR-97FS-R1, 2001. [Online]. Available: <https://www.caac.gov.cn/XXGK/XXGK/MHGZ/201511/P020151103350133392047.pdf>



YANTAO WANG received the M.Sc. degree in aeronautical materials engineering from Tianjin University, Tianjin, China, in 2008. His research interests include precise control of flight operation risk under 5G and satellite communication and 4DT track generation and conflict resolution.

He joined the Civil Aviation University of China in 2008 and currently serves as the Director of the Flight Operations Control Department, Executive Director of the China Civil Aviation Flight Operations Research Institute, Tianjin. He is also

a Special Expert of the Science and Technology Development Center of the Ministry of Education in China, a Member of the China Civil Aviation Flight Operations Expert Group, a Science and Technology Expert of Shanghai/Tianjin and other places, and an Aviation Science Expert of the Chinese Society of Aeronautics and Astronautics.



JIASHUAI LI received the B.Sc. degree in material chemistry in 2023 from the Civil Aviation University of China, Tianjin, China, where he is currently working toward the M.Sc. degree in air traffic management with the guidance of Yantao Wang and Yujie Yuan.

His research interests include urban air traffic management, route design and urban air traffic planning.



YUJIE YUAN (Member, IEEE) received the B.Sc. degree in management from Keuka College, Keuka Park, NY, USA, in 2015, the B.Sc. degree in project management from the Yunnan University of Finance and Economics, Yunnan, China, in 2015, the M.Sc. degree in science in management from the Keuka College, in 2016, and the Ph.D. degree in control system and engineering from the School of Traffic and Transportation, Beijing Jiaotong University, Beijing, China in 2023.

She is currently a Lecturer with Civil Aviation University of China, Tianjin, China. Her research interests include system engineering, transport engineering, high-speed rail and civil aviation competition, and system control.



CHUN SING LAI (Senior Member, IEEE) received the B.Eng. degree (First-Class Hons.) in electrical and electronic engineering from the Brunel University of London, London, U.K., in 2013, and the D.Phil. degree in engineering science from the University of Oxford, Oxford, U.K., in 2019. He is currently a Senior Lecturer with the Department of Electronic and Electrical Engineering, Brunel University of London. From 2018 to 2020, he was an U.K. Engineering and Physical Sciences Research Council Research Fellow with the School of Civil

Engineering, University of Leeds, Leeds, U.K.

His current research interests include power system optimization and data analytics. He was the Publications Co-Chair for both 2020 and 2021 IEEE International Smart Cities Conferences. He is the Vice Chair of the IEEE Smart Cities Publications Committee and an Associate Editor for IET Energy Conversion and Economics. He is the Working Group Chair for IEEE P2814 Standard; an Associate Vice President for Systems Science and Engineering of the IEEE SYSTEMS, Man, and Cybernetics Society; and the Chair of the IEEE SMC Intelligent Power and Energy Systems Technical Committee. He is an IET Member and a Chartered Engineer.